Online Supplement to "Matching Theory and Evidence on Covid-19 using a Stochastic Network SIR Model"

M. Hashem Pesaran

University of Southern California, USA, and Trinity College, Cambridge, UK

Cynthia Fan Yang

Florida State University

December 18, 2021

This online supplement is set out in eight sections. Section S1 reviews the literature. Section S2 establishes the classical multigroup SIR model as a linearized version of the moment conditions we have derived for our proposed model. This section also generalizes the proposed model to allow for truncated geometric recovery and provides a derivation of vaccine efficacy in the multigroup version of the model. Section S3 discusses the edge probability and how the random networks were generated in our simulation exercises. This section also compares the simulated models across different population sizes, the number of groups, and network types. Section S4 reports additional Monte Carlo results on estimation of the transmission rate and details the algorithm used to jointly estimate the transmission rate and multiplication factor. It also discusses the estimation of the recovery rate. Section S5 presents additional estimates of the reproduction numbers for selected European countries and the US. Section S6 reports further estimates of the multiplication factor for the European countries and the US. It also compares the reported total cases without and with adjustment for under-reporting. Section S7 provides results of additional counterfactual exercises. Finally, Section S8 gives the details of data sources.

S1 Related literature

Our modelling approach relates to two important strands of the literature on mathematical modelling of infectious diseases, namely the classical SIR model due to Kermack and McKendrick

(1927) and its various extensions to multigroup SIR models, and the individual-based network models. The multigroup SIR model allows for a heterogeneous population where each compartment (S, I, or R) is further partitioned into multiple groups based on one or more factors, including age, gender, location, contact patterns, and a number of economic and social factors. One of the earliest multigroup models was pioneered by Lajmanovich and Yorke (1976), who developed a class of SIS (susceptible-infected-susceptible) models for the transmission of gonorrhea. Subsequent extensions to the multigroup SIR model and its variants include Hethcote (1978), Thieme (1983, 1985), Beretta and Capasso (1986), and many others. Reviews of multigroup models can be found in Hethcote (2000) and Thieme (2013). For some of the recent contributions on the multigroup SIR models and their stability conditions, see, for example, Hyman, Li, and Stanley (1999), Guo, Li, and Shuai (2006), Li, Shuai, and Wang (2010), Ji, Jiang, and Shi (2011), Ding, Qin, and Ding (2015) and Zhou, Yang, and Zhang (2017). In contrast, we do not model the progression of epidemics at the compartment level; instead, we develop an individual-based stochastic model from which we derive a set of aggregate moment conditions. Interestingly, we are able to show that the multigroup SIR model can be derived as a linearized-deterministic version of our individual-based stochastic model.

Our analysis also relates to the more recent literature on mathematical models of epidemics on networks, whereby the spread of the epidemic is modelled via networks (or graphs), with nodes representing single individuals or groups of individuals and links (or edges) representing contacts. The adoption of networks in epidemiology has opened up a myriad of possibilities, using more realistic contact patterns to investigate the impact of network structure on epidemic outcomes and to design network-based interventions. Kiss, Miller, and Simon (2017) provide a systematic treatment of this literature, with related reviews in Miller and Kiss (2014) and Pastor-Satorras et al. (2015).

Being based on individual outcomes, our approach is more closely related to the individual-based models surveyed by Willem et al. (2017) and Nepomuceno, Resende, and Lacerda (2018). These models consider the transition probability of individuals from one state (S, I, R) to another (Rocha and Masuda, 2016; Gourieroux and Jasiak, 2020). In contrast, as noted in the introduction, we do not model the transition probabilities, but rather we model the contact probabilities

and unobserved individual-specific probability of becoming infected, and then derive individual-specific transition probabilities. Like the individual-based models, our approach also allows for considerable group heterogeneity and has the advantage that aggregates up to the multigroup SIR model.

In order to calibrate the average number of contacts in our model, we drew upon the literature on social contact patterns relevant to the transmission of respiratory infectious diseases. Before the outbreak of Covid-19, large-scale social contact surveys have been conducted in many countries aiming to guide effective policies on infectious disease control and prevention.[S1] The POLYMOD study of social contacts in eight European countries by Mossong et al. (2008) is a notable landmark.[S2] Many similar surveys have been conducted since. Among them, the contact studies in Hong Kong (Leung et al., 2017) and Shanghai (Zhang et al., 2019) provide valuable information about the pre-Covid social contacts in China. Most of these studies summarize contact patterns based on age groups, contact locations (e.g., households, schools, workplaces), and time schedules (e.g., weekdays or weekends) that can be utilized in multigroup epidemiological models. With the outbreak of Covid-19, a few recent articles reported significant changes in contact patterns. For example, Zhang et al. (2020) find that the median number of daily contacts in Wuhan went down from 7 in normal times to 2 after the Covid-19 outbreak. The median number of daily contacts in Shanghai fell from 10 to 2. Jarvis et al. (2020) find that the average daily number of contacts declined from 10.8 in normal times to 2.8 immediately after the lockdown in the UK. In all these three cases, the contact number by age flattened after the outbreak.

In this study, we propose a new method of estimating the transmission rate, β_t, using the moment conditions we derive from our stochastic network SIR model. The transmission rate is closely connected to the reproduction numbers, which are epidemiologic metrics used to measure the intensity of an infectious disease. The basic reproduction number, denoted by $\mathcal{R}_0$, is the number of new infections expected to result from one infected individual at the start of the epidemic, and within SIR models it is defined by $\mathcal{R}_0 = \beta_0/\gamma$, where β_0 is the initial transmission

[S1] Summaries of these social contact surveys are provided by Hoang et al. (2019) and Supplementary Table S1 of Leung et al. (2017).

[S2] The eight countries are Belgium, Germany, Finland, Great Britain, Italy, Luxembourg, The Netherlands, and Poland.

rate, and γ is the recovery rate. For the current Covid-19, estimates of $\mathcal{R}_0$ range between 2 to 3.[S3] Since the disease transmissibility will vary over time due to changes in immunity and/or mitigation policies, the effective reproduction number, which we denote by $\mathcal{R}_{et}$, measures the $\mathcal{R}$ number t periods after the initial outbreak. The effective $\mathcal{R}$ number is governed by the extent to which the susceptible population is shrinking and the effectiveness of mitigation policies (whether mandated or voluntary). In the single group SIR model, we have $\mathcal{R}_{et} = (1 - c_t)\,\beta_t/\gamma$, where c_t is the per capita number of infected cases at time t.

Various methods are available in the epidemiological literature to estimate the reproduction numbers at the beginning and/or in real time during epidemics, but there is no uniform framework. Estimation approaches that are data-driven and involve simplifying assumptions include the use of the number of susceptibles at endemic equilibrium, the average age at infection, the final size equation, and calculation from the intrinsic growth rate of the number of infections (Heffernan, Smith, and Wahl, 2005). Estimation of reproduction numbers based on different mathematical models are reviewed by Chowell and Nishiura (2008), Obadia, Haneef, and Boëlle (2012), and Nikbakht et al. (2019). More recent contributions focusing on estimation of reproduction numbers for the Covid-19 pandemic include Atkeson, Kopecky, and Zha (2020), Baqaee et al. (2020), Elliott and Gourieroux (2020), Fernández-Villaverde and Jones (2020), Korolev (2021), and Toda (2020).

In this study, we estimate the transmission rate using the moment conditions derived from our stochastic individual-based network SIR model. We do not use mortality data due to its unreliability,[S4] but instead, our method of moment estimation requires only data on per capita infected cases. Our estimation method is not only simple to apply but also accounts for the time-varying under-reporting of cases. It has been widely acknowledged that the reported infected cases may suffer from considerable under-reporting, especially during the early stages of the epidemic. Li et al. (2020) estimate that only 14 percent of all infections were documented in China prior to the January 23, 2020 travel restrictions. This translates to a multiplication factor (MF) of $1/0.14 \approx 7.1$. Jagodnik et al. (2020) estimate that the recorded cases were under-reported by a

[S3] A summary of published $\mathcal{R}_0$ values is provided in Table 1 of D'Arienzo and Coniglio (2020).

[S4] The recorded Covid death toll has undergone major revisions on several occasions. For example, the UK death toll was revised downwards by 5,377 on August 12, 2020, after a review concluded the daily death figure should only include deaths that had occurred within 28 days of a positive test.

factor in the range of 3 to 16 times in seven countries as of March 28, 2020.[S5] In the US, according to the study by Havers et al. (2020) led by the Centers for Disease Control and Prevention (CDC), the number of infected cases is likely to be ten times more than reported based on antibody tests from March through May 2020. A more recent study based on antibodies from the National Institutes of Health estimates that 20 million individuals in the US were infected by mid-July, 2020, about 17 million more than previously thought (Kalish et al., 2021). This implies that MF is about $20/3 \approx 6.7$. Rahmandad, Lim, and Sterman (2021) consider 92 countries through December 22, 2020, and estimate that the cumulative cases are 7.03 times the number of officially reported cases, with 10^{th}–90^{th} percentile range 3.2–18. They also find that the magnitude of under-reporting has declined over time as testing has increased. Another source of measurement errors is reporting delays. Harris (2020) estimates that in New York City, the mean delay in reporting was five days, with 15 percent of cases reported after ten or more days, from June 21–August 1, 2020. Many existing estimation methods of reproduction numbers do not allow for measurement errors and might not be robust to acknowledged under-reporting errors. For instance, the SUR estimates developed by Korolev (2021) may be biased downward if one neglects the under-reporting of confirmed cases.

Our study also contributes to a growing literature on quantitative epidemic policy analyses. We focus on two counterfactual analyses, but our model can be used in a variety of other contexts. First, we investigate the impact of different vaccination strategies in conjunction with social distancing policy on the evolution of the epidemic. Second, we study the timing of the lockdowns, comparing the spread of Covid-19 in UK and Germany in March 2020. A number of studies have used the SIR or other compartmental models to consider the effects of different intervention strategies (such as isolating the elderly, closing schools and/or workplaces, and alternating work/school schedules) by hypothetically lowering the average number of contacts of some specific age groups, and/or contact locations/schedules from normal (pre-Covid) levels. (See Acemoglu et al. (2021), Akbarpour et al. (2020), Ferguson et al. (2020), Matrajt and Leung (2020), Willem et al. (2020), among others.) Chudik, Pesaran, and Rebucci (2021) simulate the trade-off between

[S5] See Table 2 of Jagodnik et al. (2020). The seven countries considered are China, France, Italy, Spain, the US, Germany, and the UK.

flattening the epidemic curves and lessening unemployment loss under different degrees of mandatory and voluntary social distancing policies using a modified SIR model. Toda (2020) simulates the effects of different mitigation policies on epidemic curves by reducing the transmission rate in the SIR model from its initial level. Atkeson et al. (2020) investigate the impact of earlier or later mitigation measures on the death toll. Our model can be used to investigate different non-pharmaceutical interventions either by lowering the number of contacts across age groups and/or by reducing the rate of infection upon contact. To study the effect of vaccination on controlling infection, we calibrate the model parameters so that the reduction in the probability of infection matches a given vaccine efficacy. A large body of literature has extended the standard SIR models to allow for vaccination. The typical method is to add an additional compartment, V, for vaccinated individuals and model its relationship with other compartments by another differential equation. See, for example, Berkane, Harizi, and Tayebi (2021), Dashtbali and Mirzaie (2021), and Schlickeiser and Kröger (2021).

S2 Theoretical details and extensions

S2.1 Relation to the multigroup SIR model

In this section, we show that the classical multigroup SIR model given by (8)–(10) of the main paper is a linearized-deterministic version of our moment conditions. To see this, using the identity $S_{\ell t} = n_\ell - C_{\ell t}$ and $s_{\ell t} = S_{\ell t}/n_\ell$, (30) of the main paper can be expressed as

$$E\left(s_{\ell,t+1}|s_{\ell t}, \mathbf{i}_t\right) = s_{\ell t} \exp\left(-\sum_{\ell'=1}^{L} \beta_{\ell\ell'} i_{\ell' t}\right) + O\left(n^{-1}\right) \approx s_{\ell t}\left(1 - \sum_{\ell'=1}^{L} \beta_{\ell\ell'} i_{\ell' t}\right) + O\left(n^{-1}\right). \quad \text{(S.1)}$$

Let $\Delta s_{\ell,t+1} = s_{\ell,t+1} - s_{\ell t}$. Then (S.1) can be rewritten as

$$E\left(\Delta s_{\ell,t+1}|s_{\ell t}, \mathbf{i}_t\right) \approx -s_{\ell t} \sum_{\ell'=1}^{L} \beta_{\ell\ell'} i_{\ell' t} + O\left(n^{-1}\right). \quad \text{(S.2)}$$

In comparison, dividing both sides of (8) in the multigroup SIR model by n_ℓ gives

$$\Delta s_{\ell,t+1} = -s_{\ell t} \sum_{\ell'=1}^{L} \beta_{\ell\ell'} i_{\ell' t}. \quad \text{(S.3)}$$

To exactly match the deterministic expression of $s_{\ell t}$ given by (S.3) with the stochastic process given by (S.2), we can introduce either an additive or a multiplicative random error to the right-hand side of (S.3). To ensure that $s_{\ell t}$ is non-negative for all t, a multiplicative error with mean unity would be a more reasonable choice.

Turning to the recovery process, the recovery governed by (27) of the main paper matches with the deterministic recovery equation, (10), of the SIR model under a geometric recovery process. Finally, since $I_{\ell t} = n_\ell - R_{\ell t} + S_{\ell t}$, the active cases of our model also match with the infected equation, (9), of the SIR model.

S2.2 Truncated geometric model of recovery

Here we consider a generalization of the recovery model used in the main paper. Suppose that for all individuals in group ℓ ($\ell = 1, 2, \ldots, L$), the time to recovery (or infection duration), denoted by $T^*_{i\ell,t} = t - t^*_{i\ell}$, follows a truncated geometric distribution with the probability mass distribution

$$\Pr\left(T^*_{i\ell,t} = t - t^*_{i\ell}\right) = A_\ell \left(1-\gamma_\ell\right)^{t-t^*_{i\ell}}, \text{ for } t - t^*_{i\ell} = 1, 2, \ldots, \mathfrak{D}_\ell, \tag{S.4}$$

where $\mathfrak{D}_\ell$ is the maximum number of days for an individual to recover and is assumed to be the same for all individuals in group ℓ. γ_ℓ is the probability of recovery on each day if the geometric distribution is non-truncated (i.e., $\mathfrak{D}_\ell \to \infty$). A_ℓ is a normalizing constant such that

$$A_\ell \sum_{\mathfrak{s}=1}^{\mathfrak{D}_\ell} \left(1-\gamma_\ell\right)^{\mathfrak{s}} = A_\ell \left[\frac{1-\left(1-\gamma_\ell\right)^{\mathfrak{D}_\ell}}{1-\left(1-\gamma_\ell\right)}\right] = 1,$$

which yields

$$A_\ell = \frac{\gamma_\ell}{1-\left(1-\gamma_\ell\right)^{\mathfrak{D}_\ell}}. \tag{S.5}$$

Then the "hazard function", denoted by $h_\ell\left(\mathfrak{s}, \mathfrak{D}\right)$ ($\mathfrak{s} = 1, 2, \ldots, \mathfrak{D}$), defined as the probability of individuals in group ℓ recovering at time $\mathfrak{s}$ conditional on having remained infected for $\mathfrak{s}-1$ days is given by

$$\begin{aligned} h_\ell\left(\mathfrak{s}, \mathfrak{D}_\ell\right) &= \frac{\Pr\left(T^* = \mathfrak{s}\right)}{\Pr\left(T^* > \mathfrak{s}-1\right)} = \frac{\Pr\left(T^* = \mathfrak{s}\right)}{1-\Pr\left(T^* \leq \mathfrak{s}-1\right)} \\ &= \frac{A_\ell\left(1-\gamma_\ell\right)^{\mathfrak{s}-1}}{1-A_\ell\sum_{x=1}^{\mathfrak{s}-1}\left(1-\gamma_\ell\right)^x}. \end{aligned}$$

Now using (S.5) we have

$$h_\ell(\mathfrak{s}, \mathfrak{D}_\ell) = \frac{\gamma_\ell (1-\gamma_\ell)^{\mathfrak{s}-1}}{(1-\gamma_\ell)^{\mathfrak{s}-1} - (1-\gamma_\ell)^{\mathfrak{D}_\ell}}, \text{ for } \mathfrak{s} = 1, 2, \ldots, \mathfrak{D}_\ell.$$

Note that given a finite $\mathfrak{D}_\ell$ and $0 < \gamma_\ell < 1$, $h_\ell(\mathfrak{s}, \mathfrak{D}_\ell)$ monotonically increases with $\mathfrak{s}$. Hence, by assuming a truncated geometric distribution for recovery time, we are able to allow for the possibility that the longer an individual is infected, the more likely s/he will recover. It is also clear that $h_\ell(\mathfrak{s}, \mathfrak{D}_\ell) \to \gamma_\ell$ as $\mathfrak{D}_\ell \to \infty$, which establishes the familiar result for a non-truncated geometric distribution used in the main paper. Under the truncated geometric distribution, we have

$$\begin{aligned}
&E\left[\zeta_{i\ell,t+1}(t^*_{i\ell}) \,\middle|\, x_{i\ell,t}, y_{i\ell,t}, y_{i\ell,t-1}, \ldots, y_{i\ell,t^*_{i\ell}}\right] \\
&= \Pr\left[\zeta_{i\ell,t+1}(t^*_{i\ell}) = 1 \,\middle|\, x_{i\ell,t}, y_{i\ell,t} = 0, y_{i\ell,t-1} = 0, \ldots, y_{i\ell,t^*_{i\ell}} = 0\right] \\
&= h_\ell(t - t^*_{i\ell}, \mathfrak{D}_\ell),
\end{aligned}$$

and the recovery process will be given by

$$\begin{aligned}
E(R_{\ell,t+1}|R_{\ell t}, C_{\ell t}) &= R_{\ell,t} + \sum_{i=1}^{n_\ell} h_\ell(t - t^*_{i\ell}, \mathfrak{D}_\ell)(1 - y_{i\ell,t}) x_{i\ell,t} \\
&= R_{\ell,t} + \sum_{i=1}^{n_\ell} \frac{\gamma_\ell (1-\gamma_\ell)^{t-t^*_{i\ell}-1}}{(1-\gamma_\ell)^{t-t^*_{i\ell}-1} - (1-\gamma_\ell)^{\mathfrak{D}_\ell}} (1 - y_{i\ell,t}) x_{i\ell,t}, \qquad \text{(S.6)}
\end{aligned}$$

which does not simplify to the standard recovery process used in the SIR models, unless $\mathfrak{D}_\ell \to \infty$.

S2.3 Derivation of vaccine efficacy in the multigroup model

The main paper has established Eq. (56), $\mu^1/\mu^0 \approx 1/(1-\epsilon_v)$, assuming a single group model. Here we show that this result also holds in the multigroup model. Recall that

$$\begin{aligned}
E(x_{i\ell,t+1} | x_{i\ell,t} = 0, \mu_{i\ell}, \mathbf{i}_t) &= 1 - \prod_{\ell'=1}^{L} \left(1 - p_{\ell\ell'} + p_{\ell\ell'} e^{-\frac{\tau_\ell}{\mu_{i\ell}}}\right)^{I_{\ell' t}} \\
&\approx 1 - e^{\frac{\tau_\ell}{\mu_{i\ell}}\left(\sum_{\ell'=1}^{L} i_{\ell' t} k_{\ell\ell'}\right)} \approx \frac{\tau_\ell}{\mu_{i\ell}} \left(\sum_{\ell'=1}^{L} i_{\ell' t} k_{\ell\ell'}\right).
\end{aligned}$$

Using this in (54) of the main paper and letting $i^0_{\ell t}$ be the proportion of active cases in group ℓ when the vaccine is introduced, we obtain

$$\frac{\tau_\ell \sum_{\ell'=1}^{L} i^0_{\ell' t} k_{\ell\ell'}}{\mu^1} = (1 - \epsilon_v) \frac{\tau_\ell \sum_{\ell'=1}^{L} i^0_{\ell' t} k_{\ell\ell'}}{\mu^0},$$

which simplifies to $\mu^1/\mu^0 = 1/(1-\epsilon_v)$.

S3 Calibration and simulation of the model

S3.1 Generating random networks

This section describes how we generated random draws from the Erdős-Rényi and power law networks in the case of single and multigroup random networks used in our simulations.

First, in an Erdős-Rényi (ER) random graph, each edge has a fixed probability of being present or not independently of all other edges. Specifically, we generate the ER random network with n nodes and a single group by considering all possible edges and including an edge between each distinct pair of nodes with probability $p = k/(n-1)$.

Second, we generate the power law random network in the case of a single group following the standard procedure in the literature:[S6] at each time t, we first draw a degree sequence from the (truncated) power law distribution given by (S.8), and then generate a network with that degree sequence based on a configuration model.[S7] Specifically, we draw a degree sequence $k_i(t)$ randomly and independently over i for $i = 1, 2, \cdots, n$, (with replacement), such that $k_i(t)$ realizes with probability p_{k_i}. Then we generate a configuration model with the degree sequence $\{k_i(t)\}$ by the standard algorithm – first assign each node with a number of stubs (half edges) that is equal to its degree, then match two stubs uniformly at random to form an edge and continue until all stubs are matched. Since the number of edges, denoted by $m(t)$, in a graph satisfies $2m(t) = \sum_i k_i(t)$, the generated degrees must add to an even number to be able to construct a graph. If the generated degrees add to an even number, we simply throw them away and generate another sequence. Also notice that this algorithm may produce self-loops and multi-edges. This is not a concern if n is sufficiently large since the density of such problematic links is of order $O(n^{-1})$.[S8] In simulations, we discard self-loops and collapse multi-edges. The resulting graph is used as the power law contact network for time t, and the same procedure is repeated in each t

[S6] See, for example, Kiss et al. (2017), p. 20.

[S7] A configuration model is a model of a random graph with a given degree sequence. The name "configuration" originates from Bollobás (1980) meaning arrangements of edges in the model.

[S8] A proof can be found in Newman (2018), pp. 373–375.

and over replications.

It follows from the degree distribution given by (S.8) that the normalizing constant has the expression $C = \left(\sum_{k_{\min}}^{k_{\max}} x^{-\alpha}\right)^{-1}$, and then the average degree of the power law graph is

$$k = E(x) = \sum_{k_{\min}}^{k_{\max}} xp(x) = C \sum_{k_{\min}}^{k_{\max}} x^{1-\alpha} = \left(\sum_{k_{\min}}^{k_{\max}} x^{-\alpha}\right)^{-1} \left(\sum_{k_{\min}}^{k_{\max}} x^{1-\alpha}\right). \tag{S.7}$$

In simulations, the value of the exponent, α, is solved from (S.7) such that $k = 10$.

Given the degree sequence $\boldsymbol{k}(t) = [k_1(t), k_2(t), \ldots, k_n(t)]'$, the (conditional) edge probability between node i and node j in the configuration model is[S9]

$$E[d_{ij}(t) \mid \boldsymbol{k}(t)] = \frac{k_i(t) k_j(t)}{2m(t) - 1},$$

which in the limit of large $m(t)$ can be rewritten as

$$E[d_{ij}(t) \mid \boldsymbol{k}(t)] = \frac{k_i(t) k_j(t)}{2m(t)} = \frac{k_i(t) k_j(t)}{\sum_{r=1}^{n} k_r(t)} = \frac{k_i(t) k_j(t)}{nk}.$$

Since $k_i(t)$ and $k_j(t)$ are independent draws from the power law distribution with mean k, the (unconditional) edge probability is

$$p_{ij} = E[d_{ij}(t)] = E\{E[d_{ij}(t) \mid \boldsymbol{k}(t)]\} = \frac{k^2}{nk} = \frac{k}{n},$$

which is the same as the edge probability in the ER random network.

Finally, the network with multigroup can be generated following the stochastic block model (SBM), which is a popular random graph model for blocks (groups or communities) in networks.[S10] Recall our assumption that the probability of contacts is homogeneous within groups but different across groups. Node (or individual) i in group ℓ is denoted by (i, ℓ). At each time t, we draw a network in which the edge between each distinct pair of nodes, (i, ℓ) and $\left(j, \ell'\right)$, exists with probability $p_{\ell\ell'}$. That is, the edge probabilities depend on the groups to which nodes belong. We set the within-group probability $p_{\ell\ell} = k_{\ell\ell}/(n_\ell - 1) \approx k_{\ell\ell}/n_\ell$, and the between-group probability $p_{\ell\ell'} = k_{\ell\ell'}/n_{\ell'}$. By construction, we have $p_{\ell\ell'} = p_{\ell'\ell}$ under the reciprocity condition, $n_\ell k_{\ell\ell'} = n_{\ell'} k_{\ell'\ell}$. Note that if $p_{\ell\ell'} = p$ for all groups ℓ and ℓ', the SBM reduces to the ER random graph. If $p_{\ell\ell'}$ are not all identical, the SBM generates ER random graphs within each group and random bipartite

[S9] See, e.g., Newman (2018), p. 373.

[S10] A recent review of the stochastic block models is provided by Lee and Wilkinson (2019).

graphs between groups. Accordingly, the degree distribution of the generated network is a mixture of Poisson degree distributions. To create heavy-tailed degree distributions or other types of degree heterogeneity, one can generalize the SBM analogous to the configuration model or consider the degree-corrected SBM, but these generalizations are beyond the scope of the current paper.[S11]

S3.2 Simulated properties of the model

First, we consider how the simulated properties of the proposed model vary as we increase the population size, n. Specifically, we carry out simulations with $n = 10,000$, $50,000$, and $100,000$, assuming a fixed transmission rate and a single group model, where the parameters take values $k = 10$, $\gamma = 1/14$, $\mathcal{R}_0 = 3$, $\beta = \gamma\mathcal{R}_0 = 3/14$, and $\tau = \beta/k$. For each replication, the simulation is initialized with $1/1000$ of the population randomly infected on day 1. The number of replications is set to $B = 1,000$ for all experiments. Figure S.1 displays the proportions of new cases. As can be seen, the simulated cases are hardly affected by the choice of n in the range of $(10,000,$ $100,000)$. The maximum proportion of infected, $c^* = B^{-1}\sum_{b=1}^{B}\max_t c_t^{(b)}$, equals 0.94 in all three cases. The time at which new cases peak is also almost the same across n. Although uncertainty in the simulation results decreases with larger n, the interquartile range with $n = 10,000$ is quite tight.

Figure S.2 compares the simulated aggregate new cases averaged over $1,000$ replications obtained by the single group model and the multigroup model with five age groups detailed in Section 5 of the main paper. What stands out in the figure is the similarity of the epidemic outcomes, including the peak of new cases, the maximum proportion of infected, and the duration of the epidemic. This result suggests that the aggregate outcomes do not seem to be affected by the number of groups used in the simulations.

We next examine the effect of network topology on the simulation results. In particular, we consider two widely used random networks – the Erdős-Rényi (ER) and the power law random networks. For simplicity, we examine the single group model. Recall that in an ER random graph, each pair of the nodes are connected at random with a uniform probability $p = k/(n-1)$. In the limit of large n (with the mean degree k fixed), the ER random network has a Poisson

[S11] See, for example, Newman (2018), Section 12.11.16, for a discussion.

Figure S.1: Simulated number of new cases using a single group model with $\mathcal{R}_0 = 3$ under different population sizes

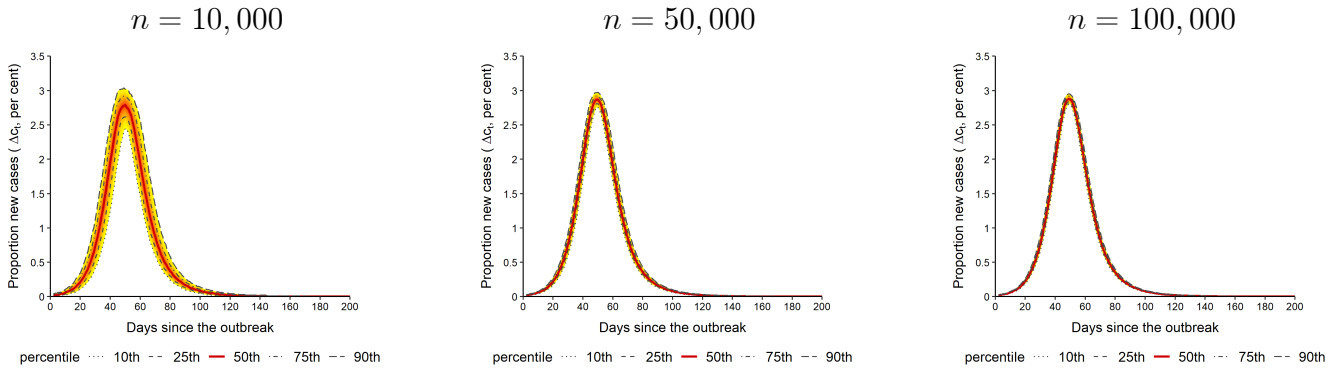

Notes: We set 1/1000 of the population randomly infected on day 1 and use the Erdős-Rényi random network with mean contact number $k = 10$. The recovery rate is $\gamma = 1/14$. The exposure intensity parameter is $\tau = \gamma\mathcal{R}_0/k$. $c^* = B^{-1}\sum_{b=1}^{B} \max_t c_t^{(b)} = 0.94$ in all three cases. The number of replications is $B = 1,000$.

degree distribution, which may depart from real-world contact networks in which a small number of individuals (such as school-aged children, medical professionals, delivery drivers, and sales workers) may have a relatively high number of daily contacts. In other words, the degree distribution of the contact networks may be heavy-tailed (right-skewed). The power law random network is a popular choice to model this phenomenon. In a (truncated) power law graph, the degree distribution follows the power-law distribution:

$$p_x = Cx^{-\alpha}, \quad x = k_{\min}, k_{\min}+1, \ldots, k_{\max}, \tag{S.8}$$

where p_x is the fraction of nodes in the graph with degree x, $k_{\min}$ ($k_{\max}$) is the minimum (maximum) degree, $\alpha > 1$ is a constant known as the power law exponent, and C is a normalization constant such that $\sum_{k_{\min}}^{k_{\max}} p_x = 1$. Figure S.3 illustrates the two networks with $n = 50$ nodes and the same average degree, $k = 10$. It is assumed that the minimum and maximum degrees of the power law network are $k_{\min} = 5$ and $k_{\max} = 49$, respectively. The networks were generated following the algorithms described in Section S3.1 of this online supplement. It can be seen from the figure that most nodes in the ER random network have comparable degrees with the mean degree of 10 approximately. In contrast, the power law network has a heavy-tailed degree distribution, and there are many small-degree nodes as well as a few highly connected nodes in the graph.

Figure S.4 compares the simulation results obtained using the two random networks with the

Figure S.2: The average number of aggregate new cases using the single- and multi-group models with $\mathcal{R}_0 = 3$

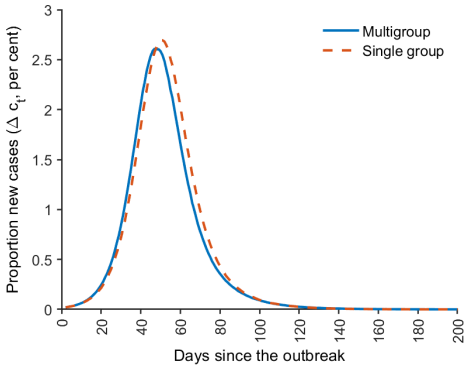

Notes: The average proportion of new cases over $1,000$ replications is displayed. The average number of new cases is very close to the median, although not shown. Population size is $n = 10,000$. In the case of a single group, the Erdős-Rényi random network with mean contact number $k = 10$ was used. $c^* = B^{-1} \sum_{b=1}^{B} \max_t c_t^{(b)} = 0.94$, and the duration of the epidemic is $T^* = 212$ days. In the case of the multigroup model, $c^* = 0.90$, and $T^* = 215$ days.

Figure S.3: Examples of Erdos-Renyi and power law networks

Erdős-Rényi random network (Truncated) power law network

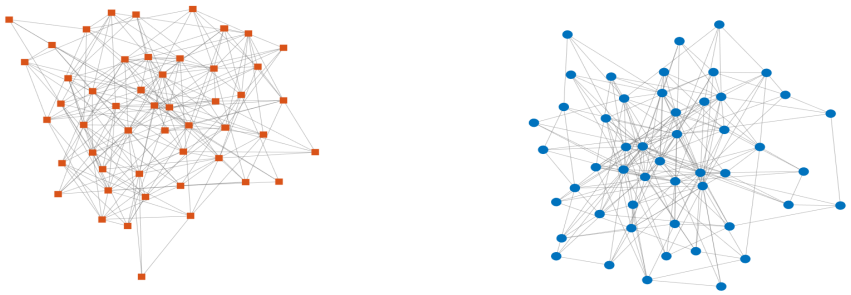

Notes: $n = 50$. Mean degree is $k = 10$ in both networks. The degree distribution in the power law network follows $p_x = Cx^{-2.43}$, for $x = 5, 6, \ldots, 49$.

same average degree of 10. We set $k_{\min} = 5$ and $k_{\max} = 50$ for the power law networks. The values of γ, $\mathcal{R}_0$, and τ, and initialization of the simulation process are as given above. We plot the proportion of new cases with uncertainty bands and the mean values across $1,000$ replications for easy comparison. It is clear from Figure S.4 that the mean epidemic curves obtained by the two different random networks overlap. Although not shown, the median simulation results are very close to the mean values for both types of networks. We therefore focus on using the random network in our simulation and calibration exercises.

Figure S.4: Simulated number of new cases using a single group model with $\mathcal{R}_0 = 3$ under different network topologies

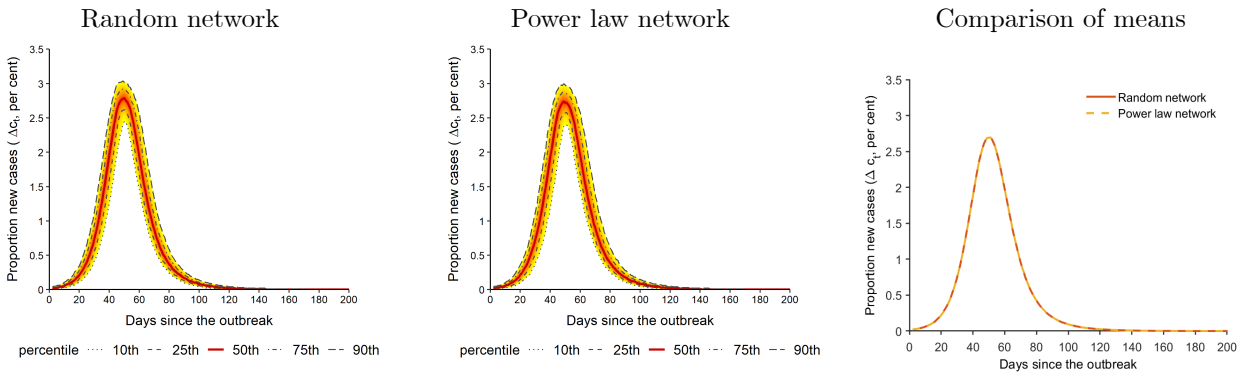

Notes: We set 1/1000 of the population randomly infected on day 1. Both networks have mean degrees $k = 10$. The recovery rate is $\gamma = 1/14$. The exposure intensity parameter is $\tau = \gamma\mathcal{R}_0/k$. Population size is $n = 10,000$. $c^* = B^{-1}\sum_{b=1}^{B} \max_t c_t^{(b)} = 0.94$ using both networks. The number of replications is $B = 1,000$.

S4 Estimation of transmission and recovery rates

S4.1 Estimation of transmission rates

This section first provides further evidence on the performance of the rolling estimators of the transmission rates assuming no measurement errors, and then describes the method that estimates the transmission rate and the multiplication factor jointly. Table S.1, which complements Table 1 in the main paper, reports the finite sample properties of the 3-weekly rolling estimates of $\mathcal{R}_0$ in the case where it is fixed at $\mathcal{R}_0 = 3$. The simulated data were obtained under the same set-up as that for Table 1, and are based on a single group model with the random network and the parameter values $k = 10$, $\gamma = 1/14$, and $\beta = 3/14$. Table S.1 presents the bias and root mean square error (RMSE) of the rolling estimates, $\hat{\mathcal{R}}_0(W) = \hat{\beta}_t(W)/\gamma$, where the window size $W = 3$ weeks, and $\hat{\beta}_t(W)$ is computed based on (49) of the main paper. The results refer to averages computed over the four non-overlapping 3-weekly sub-samples covering the $4^{th} - 15^{th}$ weeks since the outbreak.

As to be expected, the bias remains small and similar over different sub-samples. The RMSE is smaller in the middle of the epidemic than at the beginning and end stages, where i_t is very close to zero. Overall, the average RMSE of $\hat{\mathcal{R}}_0$ is reasonably small compared to the true value of

3. Compared with Table 1 of the main paper, the properties of the 2-weekly and 3-weekly rolling estimates are very close, with the 3-weekly rolling estimates having slightly smaller RMSE than the 2-weekly estimates.

Table S.1: Finite sample properties of the 3-weekly rolling estimates of $\mathcal{R}_0$, in the case where it is fixed at $\mathcal{R}_0 = 3$

		3-weekly sub-samples			
Weeks since the outbreak		$4^{th} - 6^{th}$	$7^{th} - 9^{th}$	$10^{th} - 12^{th}$	$13^{th} - 15^{th}$
Population					
$n = 10,000$	Bias	-0.0119	-0.0037	-0.0024	0.0026
	RMSE	0.0966	0.0488	0.0737	0.1687
$n = 50,000$	Bias	-0.0019	-0.0002	-0.0009	-0.0005
	RMSE	0.0395	0.0218	0.0332	0.0750
$n = 100,000$	Bias	-0.0003	0.0005	0.0000	-0.0006
	RMSE	0.0275	0.0150	0.0229	0.0544

Notes: The true value of $\mathcal{R}_0$ is set to β/γ, where $\beta = 3/14$ and $\gamma = 1/14$ so that $\mathcal{R}_0 = 3$. We fix γ and estimate β using (48) in the main paper. The number of replications is $B = 1,000$.

Next, to allow for time-varying under-reporting of cases, Section 6.2 of the main paper proposes a method that jointly estimates the transmission rate and the multiplication factor (MF). Here we give detailed steps for the joint estimation. Let $\tilde{c}^0$ denote a small threshold value and $\hat{m}_{(j)}$ denote the j^{th} estimate of MF, for $j = 1, 2, \ldots$. We propose the following algorithm.

- In the initial period of the epidemic when $\tilde{c}_t \leq \tilde{c}^0$, $t = 1, 2, \ldots, t^0$, carry out the rolling estimation of β_t with a guess value of MF. Then simulate the stochastic network model using the $\left\{\hat{\beta}_t\right\}_{t=1}^{t^0}$, and compute the first estimate of MF as the ratio of the mean calibrated cases to realized cases at the end of the initial period, namely, $\hat{m}_{(1)} = \bar{c}_{t^0}/\tilde{c}_{t^0}$, where $\bar{c}_{t^0} = B^{-1}\sum_{b=1}^{B} c_{t^0}^{(b)}$.

- When $\tilde{c}_t > \tilde{c}^0$, we jointly estimate β_t and m_t by the two equations below:

$$\hat{\beta}_t\left(W_\beta\right) = \text{Argmin}_\beta \sum_{\tau=t-W_\beta+1}^{t} \left[\frac{1 - \hat{m}_\tau(W_m)\tilde{c}_\tau}{1 - \hat{m}_{\tau-1}(W_m)\tilde{c}_{\tau-1}} - e^{-\beta\, \hat{m}_{\tau-1}(W_m)\tilde{i}_{\tau-1}}\right]^2. \tag{S.9}$$

$$\hat{m}_t(W_m) = \frac{W_m^{-1}\sum_{\tau=t-W_m+1}^{t}\left(1 - B^{-1}\sum_{b=1}^{B} e^{-\hat{\beta}_{\tau-1}\left(W_\beta\right) i_{\tau-1}^{(b)}}\right)}{W_m^{-1}\sum_{\tau=t-W_m+1}^{t}\left[\tilde{c}_\tau - \left(B^{-1}\sum_{b=1}^{B} e^{-\hat{\beta}_{\tau-1}\left(W_\beta\right) i_{\tau-1}^{(b)}}\right)\tilde{c}_{\tau-1}\right]}, \tag{S.10}$$

  where W_β and W_m are the rolling window sizes. Specifically,

– From t^0+1 to $t_2 = t^0 + W_m$, carry out rolling estimation of β_t by (S.9) using $\hat{m}_{(1)}$. Then continue the simulations using $\left\{\hat{\beta}_t\right\}_{t=t^0+1}^{t_2}$ from the stored status, and compute $\hat{m}_{(2)}$ by (S.10) at t_2.

– From t_2+1 to $t_3 = t_2 + W_m$, carry out rolling estimation of β_t by (S.9) using $\hat{m}_{(2)}$. Then continue the simulations using $\left\{\hat{\beta}_t\right\}_{t=t_2+1}^{t_3}$ and compute $\hat{m}_{(3)}$ by (S.10) at t_3.

– Continue the above steps to obtain $\hat{m}_{(4)}$, $\hat{m}_{(5)}$, ..., until the end of the sample.

In practice, MF varies slowly, and it is reasonable to consider $W_\beta = W_m = 2$ or 3 weeks. We apply the above procedure to Covid-19 data in a number of European countries and the US. The results are presented in Section 7 of the main paper and Sections S5 and S6 of this supplement.

S4.2 Estimation of the recovery rate

As noted in the main paper, with reliable data on the number of removed (recovered or dead), the recovery rate, γ, can be estimated using the moment condition given by (29) of the main paper. In reality, however, it is hard to measure R_t accurately. We do not estimate γ in the calibration exercise because the data on recovery are either unavailable or problematic in the countries we considered. In the current section, we demonstrate that the recovery rate can be estimated very precisely using simulated data. To simplify the exposition, we consider a single group ($L = 1$) and suppose that the time to recovery follows a geometric distribution as in the standard SIR model. The same aggregate outcome follows in the multigroup case if the probability of recovery is the same across all groups. Under these conditions, the aggregate moment condition for recovery can be written as

$$\Delta R_{t+1} = \gamma I_t + u_{n,t+1}, \tag{S.11}$$

where $\Delta R_{t+1} = R_{t+1} - R_t$ and $u_{n,t+1}$ is a martingale difference process with respect to I_t and R_t. ($I_t = C_t - R_t$). Recall from (5) and (6) of the main paper that $R_t = \sum_{i=1}^n y_{it}$ and $I_t = \sum_{i=1}^n z_{it}$, we note that $u_{n,t+1}$ is an aggregated error, namely, $u_{n,t+1} = \sum_{i=1}^n u_{i,t+1}$. Dividing both sides of (S.11) by n yields

$$\Delta r_{t+1} = \gamma i_t + \bar{u}_{n,t+1}, \tag{S.12}$$

Table S.2: Finite sample properties of the rolling estimates of γ

		3-weekly sub-samples			
Weeks since the outbreak		$4^{th}-6^{th}$	$7^{th}-9^{th}$	$10^{th}-12^{th}$	$13^{th}-15^{th}$
2-weekly rolling estimates					
Population					
$n=10,000$	Bias($\times$100)	0.0917	0.0111	0.0040	0.0072
	RMSE($\times$100)	0.9077	0.2465	0.1315	0.1833
$n=50,000$	Bias($\times$100)	0.0247	0.0006	0.0000	0.0023
	RMSE($\times$100)	0.3716	0.1034	0.0602	0.0840
$n=100,000$	Bias($\times$100)	0.0116	0.0012	-0.0002	0.0008
	RMSE($\times$100)	0.2536	0.0730	0.0430	0.0601
3-weekly rolling estimates					
Population					
$n=10,000$	Bias($\times$100)	0.0495	0.0082	0.0041	0.0067
	RMSE($\times$100)	0.5614	0.1681	0.1104	0.1639
$n=50,000$	Bias($\times$100)	0.0092	-0.0019	0.0005	0.0020
	RMSE($\times$100)	0.2302	0.0713	0.0511	0.0760
$n=100,000$	Bias($\times$100)	0.0055	0.0008	-0.0002	0.0009
	RMSE($\times$100)	0.1589	0.0512	0.0366	0.0542

Notes: The true value of γ is 1/14. The estimating equation is given by (S.12). The number of replications is $1,000$.

where $\Delta r_{t+1}=r_{t+1}-r_t$, $r_t=R_t/n$, $i_t=I_t/n$ and $\bar{u}_{n,t+1}=n^{-1}\sum_{i=1}^{n}u_{i,t+1}$. For sufficiently large n and assuming that the individual differences in recovery are cross-sectionally weakly correlated, we have $\bar{u}_{t+1}=O_p(n^{-1/2})$. It follows that γ can be consistently estimated from (S.12) by ordinary least squares (OLS) regression of Δr_{t+1} on i_t. Note that T is finite as $n\to\infty$. Due to the presence of $O_p\left(n^{-1/2}\right)$ in (S.12), it is expected that as n increases, the randomness will diminish and estimates of γ become increasingly precise. In the limit we would expect $\Delta r_{t+1}-\gamma i_t=O_p(n^{-1/2})$.

To examine the finite sample properties of the OLS estimator of γ, we simulate our model assuming a homogeneous recovery rate and compute the aggregate time series for $B=1,000$ replications under a given population size, n. Denote the recovery and infection time series of the b^{th} replication by $r_{t+1}^{(b)}$ and $i_t^{(b)}$, respectively, for $b=1,2,\ldots,B$. For each replication, we obtain $\hat{\gamma}^{(b)}$ by regressing $\Delta r_{t+1}^{(b)}$ on $i_t^{(b)}$, without an intercept. The true value of γ in the experiment is set to 1/14.

Table S.2 reports the bias and RMSE of the OLS estimator of γ averaged over the four non-

overlapping 3-weekly sub-samples during the $4^{th} - 15^{th}$ weeks after the outbreak. Even though the bias and RMSE in the table have been multiplied by 100, they are very small in magnitude. It is evident that we can estimate γ very precisely even with short time series samples and population size $n = 10,000$. The RMSE declines as n increases, lending support to the theory. As in the case of estimating the transmission rates, the RMSEs are relatively larger in the early and late stages of the epidemic when i_t is small. The 2-weekly and 3-weekly estimates are similar, with the 3-weekly estimator having some improvement as the outbreak amplifies into an epidemic.

S5 Estimates of the effective reproduction numbers

S5.1 Estimates for selected European countries

This section provides additional estimation results of the effective reproduction numbers ($\mathcal{R}_{et}$) and transmission rates (β_t) for the six European countries considered in the main paper. First, Figure S.5 presents the realized daily new cases (7-day average per 100,000 people) and the 2-weekly rolling estimates of the transmission rates assuming a fixed MF = 3 and 5. It can be seen that the estimates of the transmission rate under different values of MF are virtually the same when c_t is small. This observation clearly shows that MF is not identified in the early stage of the epidemic. It is also clear that the daily number of infections rapidly rises when β_t is high.

To illustrate the relationship between the transmission rate and the effective reproduction number, Figure S.6 plots $\hat{\beta}_t/\gamma$ together with $\hat{\mathcal{R}}_{et} = (1 - \hat{m}_t\tilde{c}_t)\,\hat{\beta}_t/\gamma$ for the six countries, where $\hat{\beta}_t$ and $\hat{m}_t$ were estimated jointly using 2-weekly rolling windows. The values of $\hat{\mathcal{R}}_{et}$ and $\hat{m}_t$ are displayed in Figures 2 and 3 of the main paper. It is worth noting that $\hat{\mathcal{R}}_{et}$ is almost the same as $\hat{\beta}_t/\gamma$ in the early stage of the epidemic, since the proportion of infected is very small even after taking account of under-reporting. As infected cases grow, small differences between $\hat{\beta}_t/\gamma$ and $\hat{\mathcal{R}}_{et}$ start to become visible.

Figure S.7 compares the 2- and 3-weekly rolling estimates of $\mathcal{R}_{et}$ obtained by the joint estimation procedure. It is apparent that using 2- and 3-weekly rolling windows produces very similar results. Therefore, our conclusions are unaltered if we adopt the 3-weekly estimates of the

Figure S.5: Realized new cases and two-weekly rolling estimates of the transmission rates for selected European countries

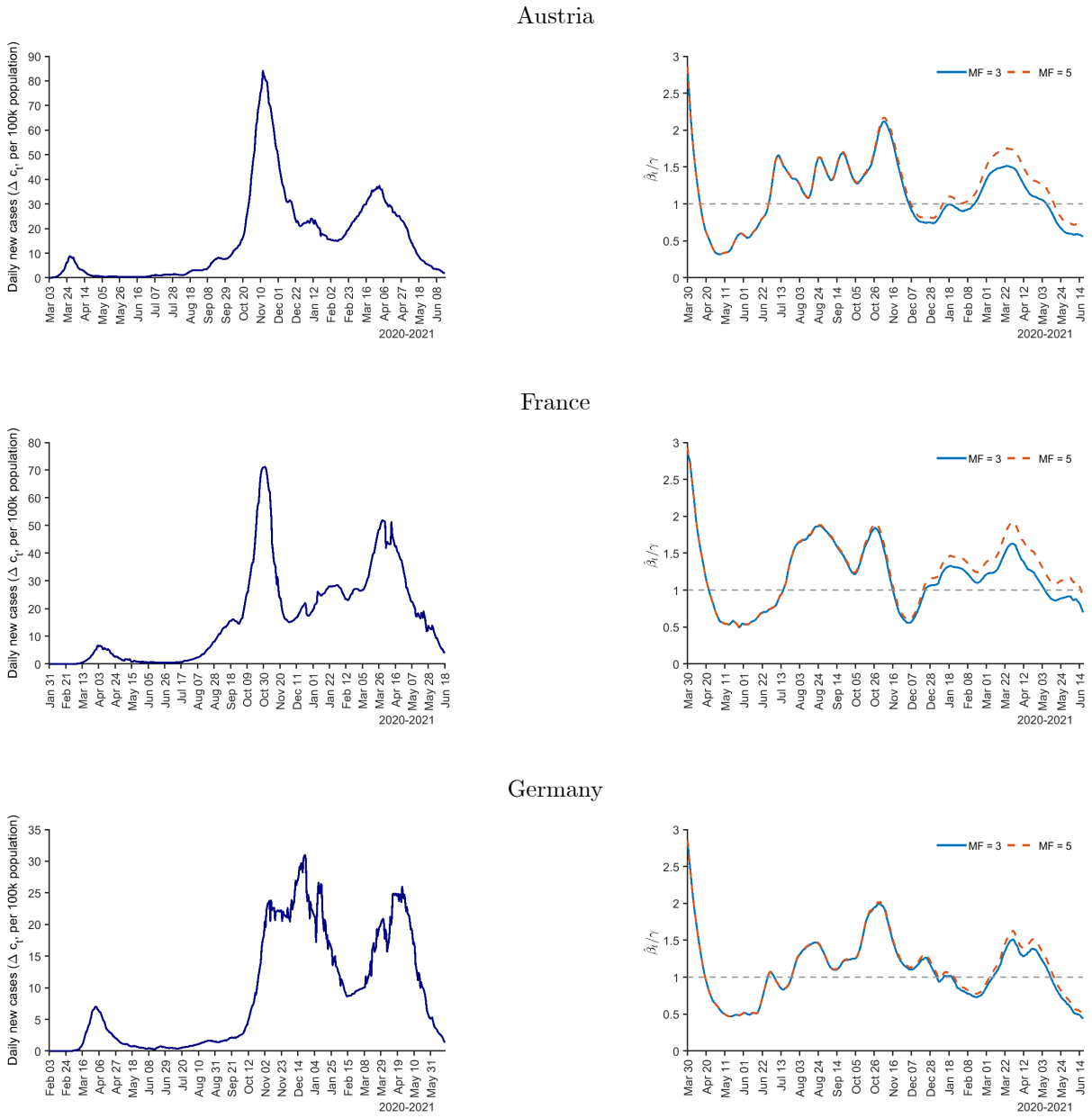

Notes: The figure plots the 7-day moving average of the reported number of new cases per 100k population and the 2-weekly rolling estimates of the transmission rate, β_t/γ, where $\gamma = 1/14$ and the multiplication factor (MF) is fixed at 3 and 5.

Figure S.5: (Continued) Realized new cases and two-weekly rolling estimates of the transmission rate for selected European countries

Italy

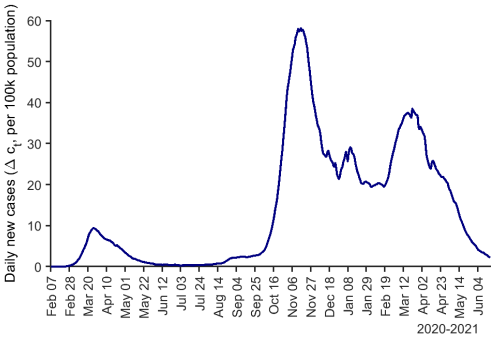

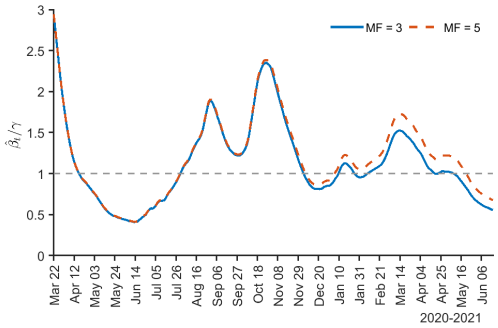

Spain

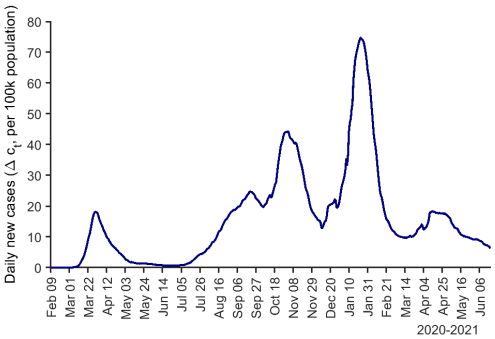

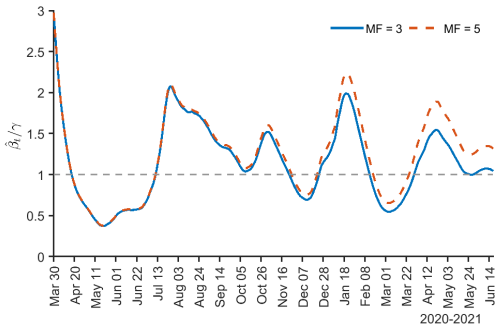

UK

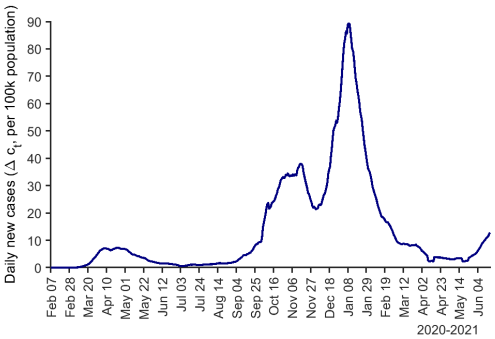

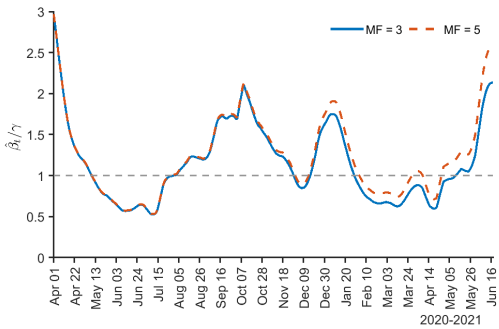

Figure S.6: Comparison of $\hat{\mathcal{R}}_{et}$ and $\hat{\beta}_t/\gamma$ for selected European countries

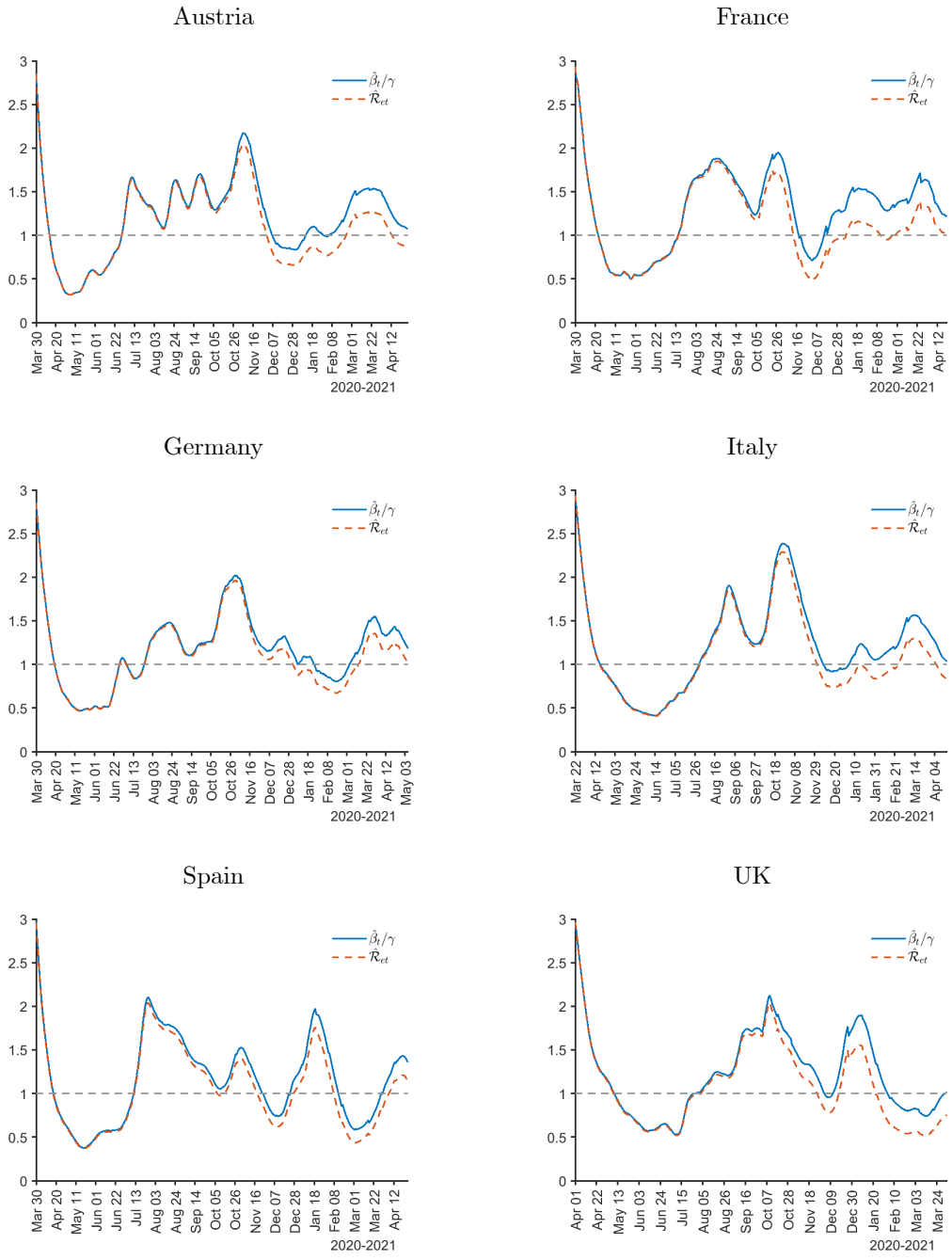

Notes: $\hat{\mathcal{R}}_{et} = (1 - \hat{m}_t \tilde{c}_t)\, \hat{\beta}_t/\gamma$, where $\tilde{c}_t$ is the reported number of infections per capita and $\gamma = 1/14$. $W_\beta = W_m = 2$ weeks. The joint estimation starts when $\tilde{c}_t > 0.01$. The initial guess estimate of the multiplication factor is 5. The simulation uses the single group model with the random network and population size $n = 50,000$. The number of replications is 500. The number of removed (recoveries + deaths) is estimated recursively using $\tilde{R}_t = (1 - \gamma)\, \tilde{R}_{t-1} + \gamma \tilde{C}_{t-1}$ for all countries, with $\tilde{C}_1 = \tilde{R}_1 = 0$.

Figure S.7: Rolling estimates of the effective reproduction numbers ($\mathcal{R}_{et}$) using the 2- and 3-weekly rolling windows for selected European countries

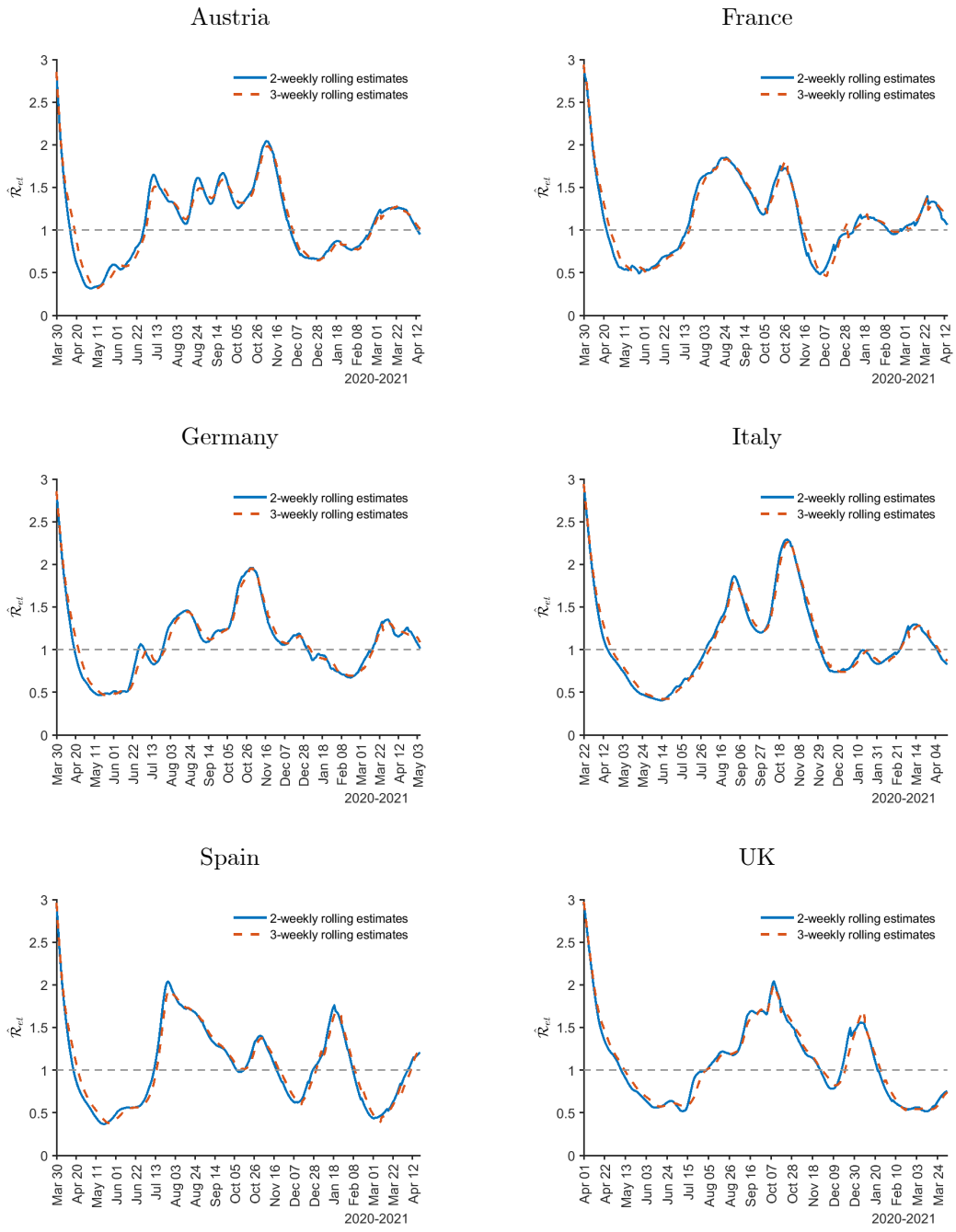

Notes: $\hat{\mathcal{R}}_{et} = (1 - \hat{m}_t \tilde{c}_t)\, \hat{\beta}_t / \gamma$, where $\tilde{c}_t$ is the reported number of infections per capita and $\gamma = 1/14$. $W_\beta = W_m = 2$ and 3 weeks. The joint estimation starts when $\tilde{c}_t > 0.01$. The initial guess estimate of the multiplication factor is 5. The simulation uses the single group model with the random network and population size $n = 50,000$. The number of replications is 500. The number of removed (recoveries + deaths) is estimated recursively using $\tilde{R}_t = (1 - \gamma)\, \tilde{R}_{t-1} + \gamma \tilde{C}_{t-1}$ for all countries, with $\tilde{C}_1 = \tilde{R}_1 = 0$.

transmission rates in calibrating the model to the empirical evidence.

S5.2 Estimates for the US

It is also interesting to examine how the reproduction numbers have evolved in the US. This section presents estimates of $\mathcal{R}_{et}$ for the US at the country and state levels. Figure S.8 presents the reported daily new cases (per 100,000 people) and the 2-weekly rolling estimates of $\mathcal{R}_{et}$ obtained by the joint estimation method for the US over the period of March 2020 to March 10, 2021 (when the share of the population fully vaccinated reached 10 percent). The results show that $\hat{\mathcal{R}}_{et}$ briefly dipped below 1 in May and then again in August 2020. In contrast with the estimates in the European countries, $\mathcal{R}_{et}$ in the US never decreased to a level as low as 0.5, resulting in a higher number of cases per capita.

Figure S.8: Realized new cases and two-weekly rolling estimates of the effective reproduction numbers ($\mathcal{R}_{et}$) for the US

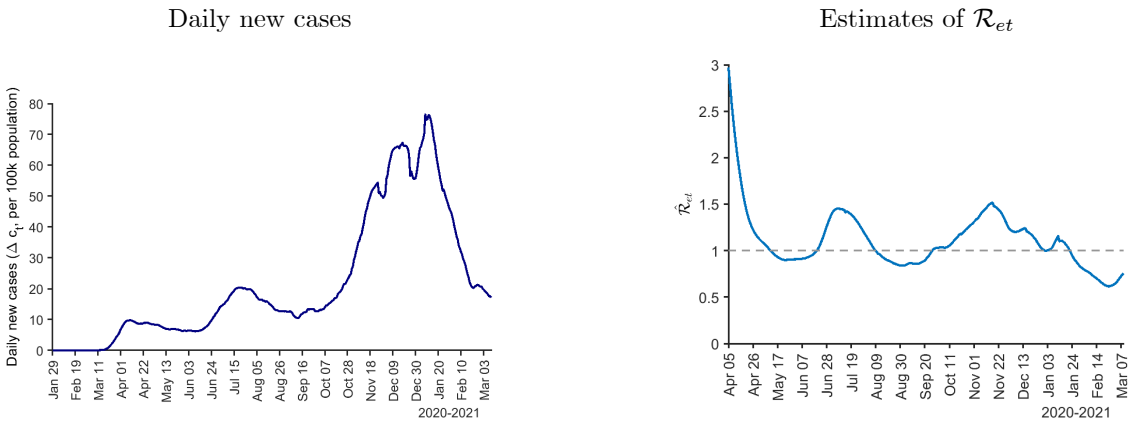

Notes: The reported daily new cases (7-day moving average) are displayed on the left. $\hat{\mathcal{R}}_{et} = (1 - \hat{m}_t \tilde{c}_t)\, \hat{\beta}_t / \gamma$, where $\tilde{c}_t$ is the reported number of infections per capita and $\gamma = 1/14$. $W_\beta = W_m = 2$ weeks. The joint estimation starts when $\tilde{c}_t > 0.01$. The initial guess estimate of the multiplication factor is 5. The simulation uses the single group model with population size $n = 50,000$. The number of replications is 500. The number of removed (recoveries + deaths) is estimated recursively using $\tilde{R}_t = (1 - \gamma)\, \tilde{R}_{t-1} + \gamma \tilde{C}_{t-1}$, with $\tilde{C}_1 = \tilde{R}_1 = 0$.

Figure S.9 presents the 2-weekly rolling estimates of $\mathcal{R}_{et}$ for the 48 contiguous states and the District of Columbia over the period March 2020 to August 7, 2021. For simplicity, we used a fixed MF = 3 in the estimation.[S12] It can be seen that the estimates share similar comovements

[S12] Some states had large-scale retrospective reporting or correction that resulted in drastic changes in the estimates. See the figure notes and also the readme file at the CSSE repository for more details.

but also display interesting patterns of heterogeneity across states. Overall, we observe that $\mathcal{R}_{et}$ rises above one around July and November 2020 and then increases quite rapidly again in July 2021 in most states. The peaks of the estimates were largely around 1.5–1.7 in the first two hikes. In contrast, the latest surge in $\mathcal{R}_{et}$ was very rapid, reaching nearly two in most states in early August. This newest wave occurred right after many states had brought down $\mathcal{R}_{et}$ to 0.5, the lowest level for many places in the US since the pandemic began.

Figure S.9: Two-weekly rolling estimates of the effective reproduction numbers ($\mathcal{R}_{et}$) for the contiguous US, by state

Notes: $\hat{\mathcal{R}}_{et} = (1 - \text{MF}\tilde{c}_t)\,\hat{\beta}_t/\gamma$, where MF = 3, $\tilde{c}_t$ is the reported number of infections per capita, and $\gamma = 1/14$. The number of removed (recoveries + deaths) is estimated recursively using $\tilde{R}_t = (1-\gamma)\,\tilde{R}_{t-1} + \gamma\tilde{C}_{t-1}$ for all states, with $\tilde{C}_1 = \tilde{R}_1 = 0$. Alabama included 306, 4,877, and 1,235 backlogged cases on May 13–15, 2021.

Figure S.9: (Continued) Two-weekly rolling estimates of the effective reproduction numbers ($\mathcal{R}_{et}$) for the contiguous US, by state

Notes: Florida stopped publishing daily case numbers on June 7, 2021. Georgia added 29,937 antigen positive cases on November 3, 2020.

Figure S.9: (Continued) Two-weekly rolling estimates of the effective reproduction numbers ($\mathcal{R}_{et}$) for the contiguous US, by state

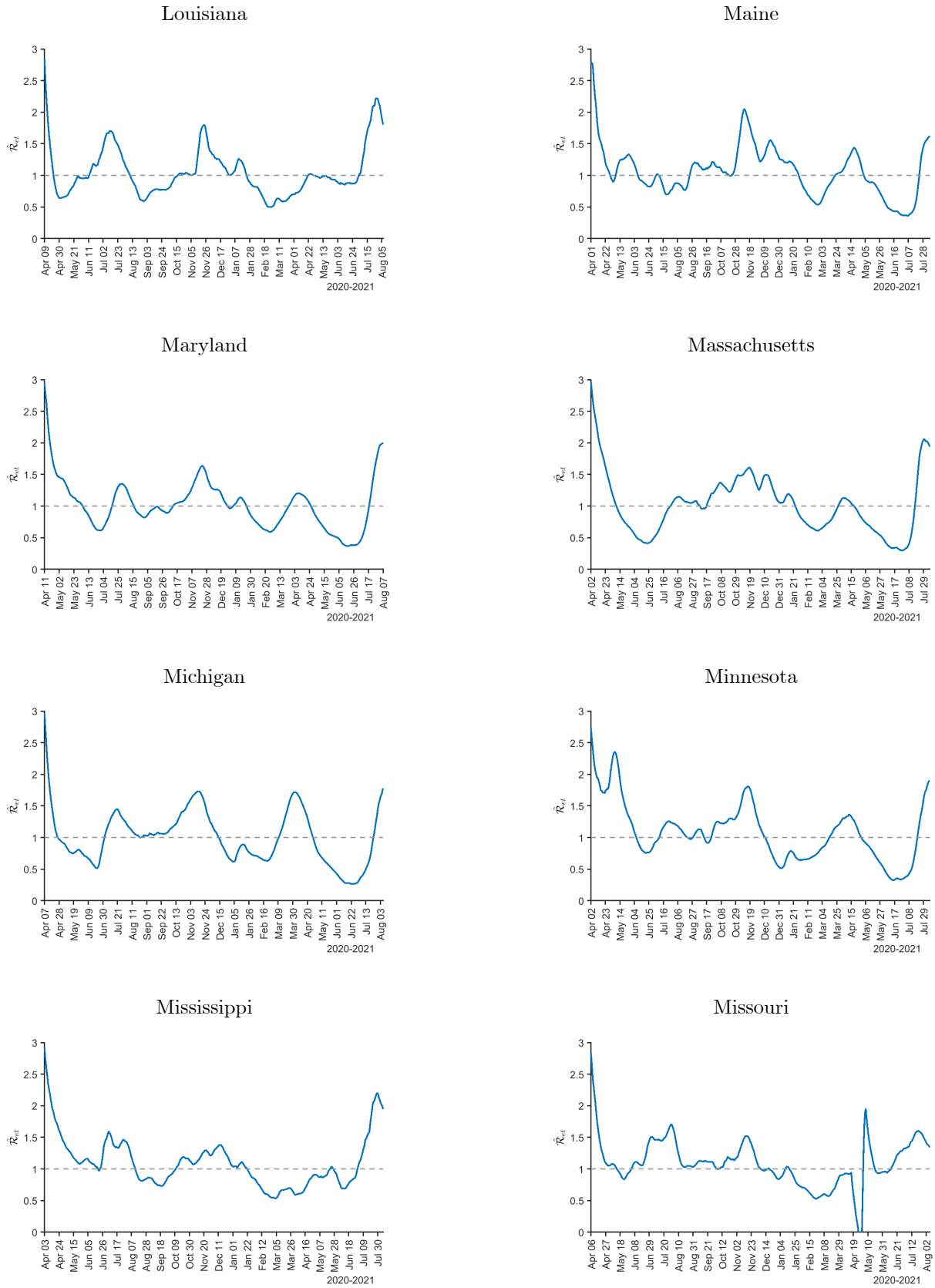

Notes: Missouri removed 11,454 double counted cases on April 17, 2021.

Figure S.9: (Continued) Two-weekly rolling estimates of the effective reproduction numbers ($\mathcal{R}_{et}$) for the contiguous US, by state

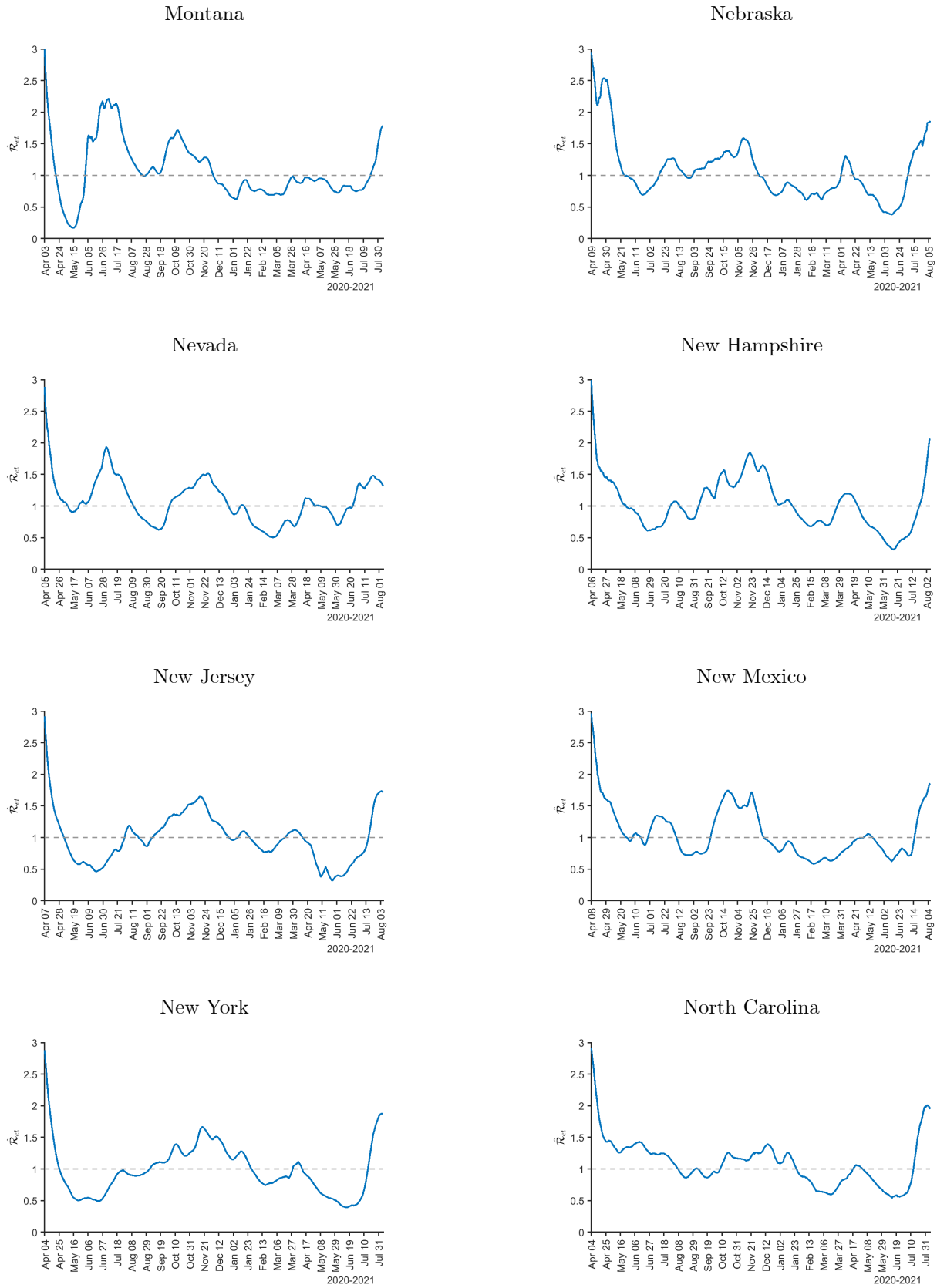

Figure S.9: (Continued) Two-weekly rolling estimates of the effective reproduction numbers ($\mathcal{R}_{et}$) for the contiguous US, by state

Notes: Ohio stopped publishing daily case numbers on June 2, 2021.

Figure S.9: (Continued) Two-weekly rolling estimates of the effective reproduction numbers ($\mathcal{R}_{et}$) for the contiguous US, by state

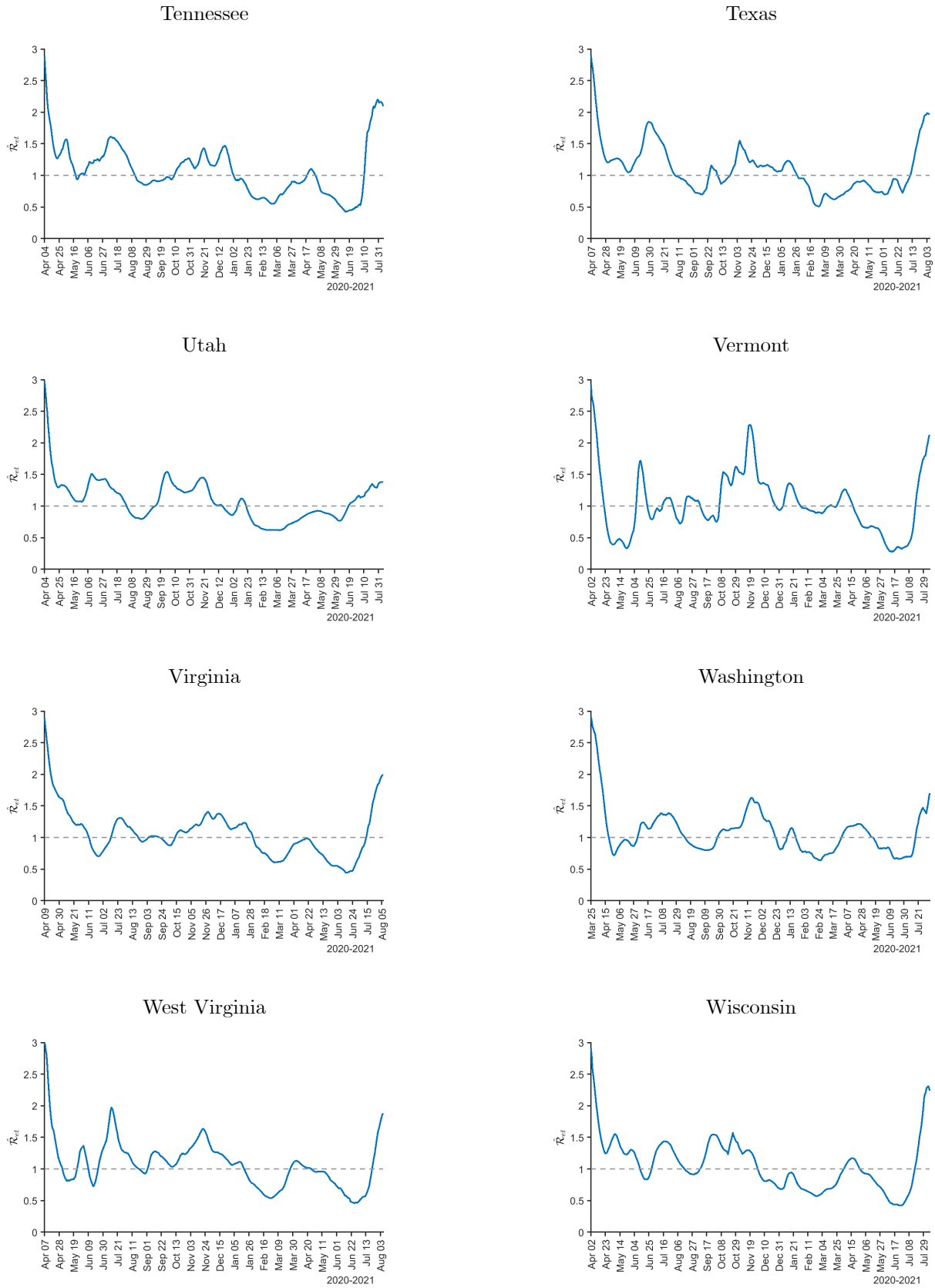

Figure S.9: (Continued) Two-weekly rolling estimates of the effective reproduction numbers ($\mathcal{R}_{et}$) for the contiguous US, by state

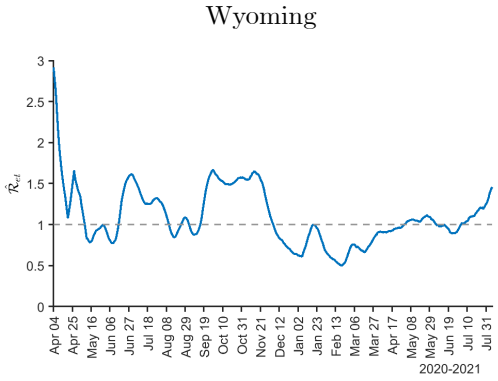

S6 Estimates of the multiplication factor

This section presents additional estimation results of the multiplication factor for the selected European countries and the US. It also compares the number of cases per capita with and without adjusting for under-reporting.

Figure S.10 compares the 2- and 3-weekly estimates of MF for the six European countries considered in the main paper. As the figure shows, the 3-weekly estimates of MF are slightly higher than the 2-weekly estimates. Still, overall they are very close and lead to negligible differences in the estimates of transmission rates, as we have seen in Figure S.7.

It is interesting to compare the reported number of total cases with the case numbers after adjusting for under-reporting using the 2-weekly estimates of the MF, which are displayed in Figure 3 of the main paper. Figure S.11 plots the 7-day moving average of infected cases (per $100,000$ people) for the six countries using the more recent data as of August 5, 2021. The left panel displays the raw data. The right panel shows the MF-adjusted total cases computed by accumulating $\hat{m}_t \times \Delta\tilde{c}_t$ from the start of the epidemic, where the MF estimates, $\hat{m}_t$, was updated every two weeks with values in between obtained by linear interpolation, and $\Delta\tilde{c}_t$ is the reported number of daily new cases (per 100k population). The MF is fixed at the last estimate for the period after the joint estimation ends.[S13] The figure clearly shows that it is important to adjust

[S13] We also considered stopping the joint estimation when the share of the population fully vaccinated reaches 15 percent. The results are quite similar and available upon request.

Figure S.10: Rolling estimates of the multiplication factor using the 2- and 3-weekly rolling windows for selected European countries

Notes: See the notes to Figure S.7.

Figure S.11: Total number of infected cases for selected European countries, without and with adjusting for under-reporting

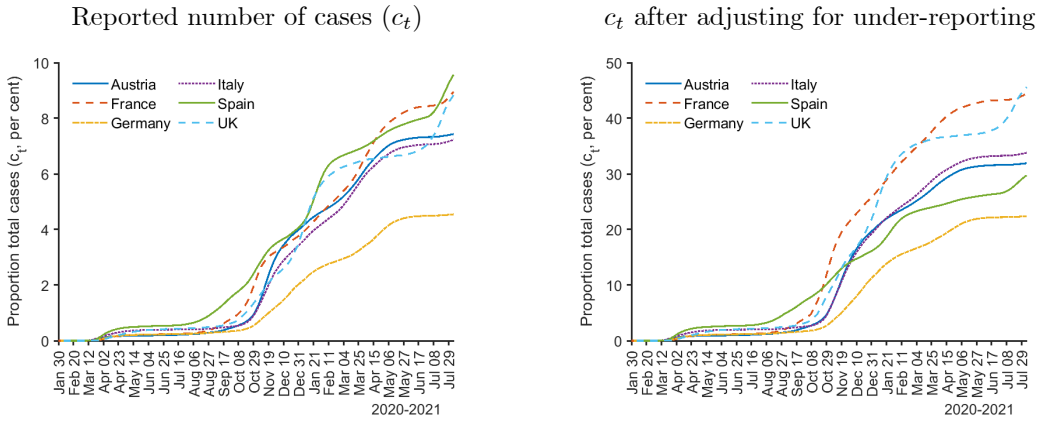

Notes: All series are 7-day moving averages. The figure on the right shows the adjusted number of total cases computed by accumulating $\hat{m}_t \times \Delta\check{c}_t$ from the outbreak to August 5, 2021, where the multiplication factor, m_t, was updated every two weeks with values in between obtained by linear interpolation.

the case counts over time by the time-varying MF. We find that, as of August 5, 2021, the number of total cases may be underestimated by three times in Spain, four times in Austria, and five times in the other four countries. After adjusting for under-reporting, we see that Spain ranks fifth in the case rate instead of first. France and the UK have the highest number of cases per capita after adjustment among these countries, approaching 40 percent in comparison to 8 percent without adjustment. In contrast, Germany did the best job controlling the total cases even after taking under-reporting into account.

We next turn to the estimates of MF for the US. The left panel of Figure S.12 presents the 2-weekly estimates of MF obtained by the joint estimation method over the period of March 2020 to March 2021 (when the share of the population fully vaccinated reached 10 percent). The results show that the estimated MF gradually declined from 7 to 3 from July 2020 to March 2021. This finding is in line with an estimate of 7 times under-reporting by mid-July in the US based on antibody tests (Kalish et al., 2021). The right panel of Figure S.12 shows the calibrated new cases compared with the realized cases that have been multiplied by the estimated MF. We can immediately observe that the calibrated cases match the several waves of Covid in the US reasonably well.

Figure S.12: Estimates of the multiplication factor and comparison of realized and calibrated new cases for the US

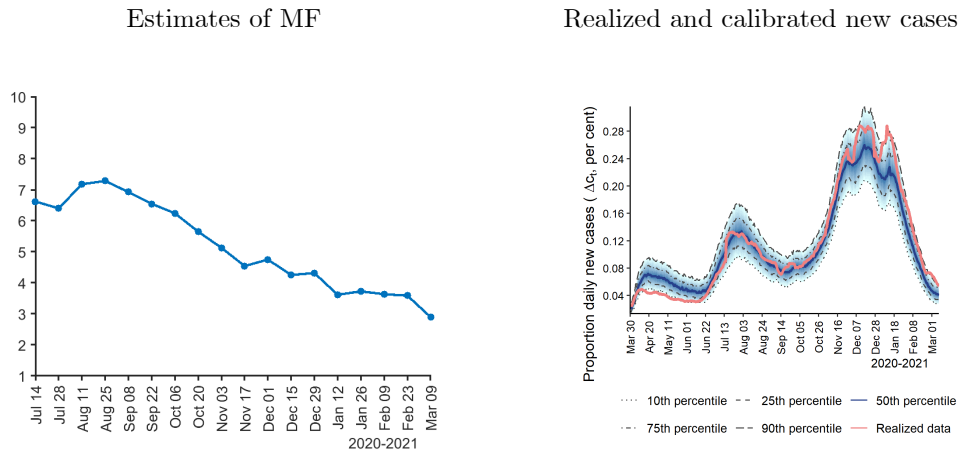

Notes: $\hat{\mathcal{R}}_{et} = (1 - \hat{m}_t \tilde{c}_t)\, \hat{\beta}_t/\gamma$, where $\tilde{c}_t$ is the reported number of infections per capita and $\gamma = 1/14$. $W_\beta = W_m = 2$ weeks. The joint estimation starts when $\tilde{c}_t > 0.01$. The initial guess estimate of the multiplication factor is 5. The simulation uses the single group model with population size $n = 50,000$. The number of replications is 500. The number of removed (recoveries + deaths) is estimated recursively using $\tilde{R}_t = (1-\gamma)\, \tilde{R}_{t-1} + \gamma \tilde{C}_{t-1}$, with $\tilde{C}_1 = \tilde{R}_1 = 0$. Realized series (7-day moving average) multiplied by the estimated multiplication factor is displayed in red.

S7 Additional counterfactual exercises

S7.1 Social distancing and vaccination

This section presents the results of additional counterfactual experiments of social distancing and vaccination. We consider the same social distancing policy as described in the main paper: the (scaled) transmission rate, β_t/γ, equals 3 in the first two weeks, falls to 0.9 linearly over the next three weeks, and remains at 0.9 for eight weeks. When social distancing is relaxed, the transmission rate increases to 1.5 linearly over the next three weeks and remains at 1.5 afterward. Figure S.13 displays the time profile of the transmission rate under this social distancing policy.

Figure S.14 complements Figure 5 of the main paper and presents additional simulation outcomes under different vaccination coverages, start times, speeds of delivery, and vaccine efficacies under the random vaccination scheme. Specifically, Figure S.14(a) displays the simulated new cases under 50 and 75 percent vaccination coverages, which are assumed to take 8 and 12 weeks, respectively. The epidemic lasts much longer if the vaccine uptake is lower, although the number

Figure S.13: Time profile of the transmission rate under social distancing

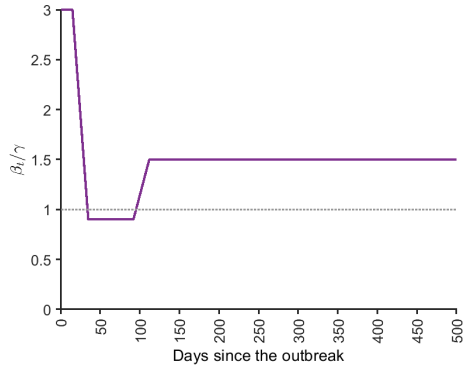

of daily new cases and total cases end up very similar. In both cases, the second epidemic wave is successfully prevented. Two important reasons are that the vaccination started early enough (during the last month of social distancing), and the vaccine is highly effective. If the vaccination begins at the end of social distancing (as shown in Figure S.14(b)), there will be a resurgence of cases, resulting in a longer duration of the epidemic and a greater number of total cases. Figure S.14(c) shows that if 75 percent of the population gets vaccinated over 8 rather than 12 weeks, the epidemic could end within 200 days, and there will not be any uptick in new cases when the social distancing is relaxed. Finally, Figure S.14(d) shows that if the vaccine has 66 percent efficacy instead of 95 percent, one would expect to see a small second wave of cases, and the epidemic would last for 65 days longer.[S14]

Figure S.15 compares the simulated group-specific and aggregate outcomes under random vaccination and vaccination in decreasing age order. It is assumed that 50 percent of the population is vaccinated over 8 weeks, as opposed to 75 percent vaccinated over 12 weeks as considered in the main paper. Comparing Figure S.15 with Figure 6 of the main paper reveals that if the vaccine coverage is lower, prioritizing the elderly would lead to a much higher level of infections for the younger age groups. The proportions of infected in Groups 2 and 3 could reach 24 and 23 percent, respectively. The age-based vaccination would also substantially increase the duration of the epidemic from 233 to 380 days if the vaccine coverage decreases from 75 to 50 percent. By

[S14]The Pfizer-BioNTech, Moderna, and Johnson & Johnson vaccines reported efficacy rates of 95%, 94.1%, and 66.3%, respectively, in preventing symptomatic Covid-19 infection (Oliver et al., 2020, 2021, and 2021).

Figure S.14: Simulated average number of new cases for different random vaccination experiments, with the same social distancing policy

(a) Comparing different vaccination coverages

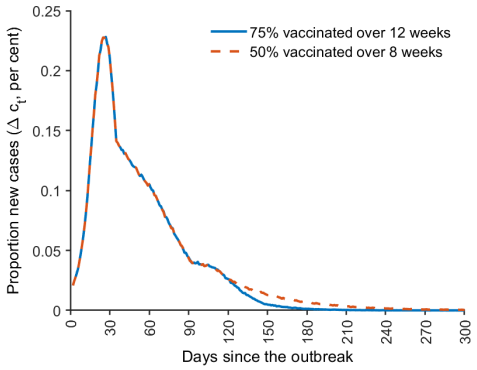

Notes: The average number of new cases over $B = 1,000$ replications is displayed. Population size is $n = 10,000$. The time profile of β_t/γ under social distancing is displayed in Figure S.13. The vaccination starts during the last month of social distancing (i.e., the 10^{th} week after the outbreak). The vaccine efficacy is $\epsilon_v = 0.95$. If 75 percent of the population is randomly vaccinated over 12 weeks, $c^* = B^{-1}\sum_{b=1}^{B} \max_t c_t^{(b)} = 0.12$, and the duration of the epidemic is $T^* = 215$ days. If 50 percent of the population is randomly vaccinated over 8 weeks, $c^* = 0.12$, and $T^* = 270$ days.

(b) Comparing different vaccination start times

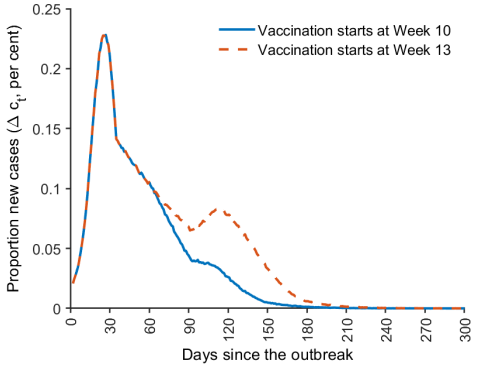

Notes: The average number of new cases over $B = 1,000$ replications is displayed. Population size is $n = 10,000$. The time profile of β_t/γ under social distancing is displayed in Figure S.13. The vaccine efficacy is $\epsilon_v = 0.95$. 75 percent of the population is randomly vaccinated over 12 weeks. If the vaccination starts during the last month of social distancing (i.e., the 10^{th} week after the outbreak), $c^* = B^{-1}\sum_{b=1}^{B} \max_t c_t^{(b)} = 0.12$, and the duration of the epidemic is $T^* = 215$ days. If the vaccination starts at the end of social distancing (i.e., the 13^{th} week after the outbreak), $c^* = 0.15$, and $T^* = 248$ days.

Figure S.14: (Continued) Simulated average number of new cases for different random vaccination experiments, with the same social distancing policy

(c) Comparing different vaccination speeds

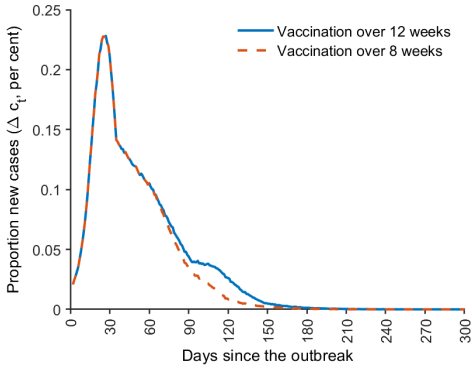

Notes: The average number of new cases over $B = 1,000$ replications is displayed. Population size is $n = 10,000$. The time profile of β_t/γ under social distancing is displayed in Figure S.13. The vaccination starts during the last month of social distancing (i.e., the 10^{th} week after the outbreak). The vaccine efficacy is $\epsilon_v = 0.95$. 75 percent of the population is randomly vaccinated. If the vaccination is administered over 12 weeks, $c^* = B^{-1}\sum_{b=1}^{B} \max_t c_t^{(b)} = 0.12$, and the duration of the epidemic is $T^* = 215$ days. If the vaccination is administered over 8 weeks, $c^* = 0.11$, and $T^* = 197$ days.

(d) Comparing different vaccine efficacies

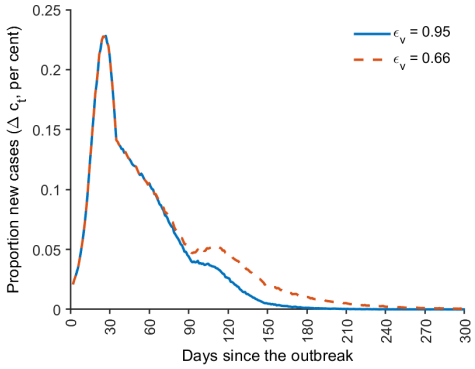

Notes: The average number of new cases over $B = 1,000$ replications is displayed. Population size is $n = 10,000$. The time profile of β_t/γ under social distancing is displayed in Figure S.13. The vaccination starts during the last month of social distancing (i.e., the 10^{th} week after the outbreak). 75 percent of the population is randomly vaccinated over 12 weeks. If the vaccine efficacy is $\epsilon_v = 0.95$, $c^* = B^{-1}\sum_{b=1}^{B} \max_t c_t^{(b)} = 0.12$, and the duration of the epidemic is $T^* = 215$ days. If $\epsilon_v = 0.66$, then $c^* = 0.13$, and $T^* = 280$ days.

Figure S.15: Simulated average number of group-specific and aggregate new cases, assuming social distancing combined with random vaccination or vaccination in decreasing age order

Group 1: [0, 15)

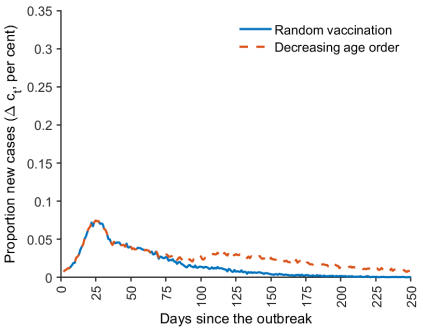

Random: $c_1^* = 0.04$
By age: $c_1^* = 0.07$

Group 2: [15, 30)

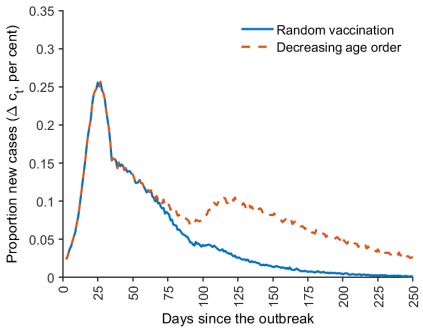

Random: $c_2^* = 0.14$
By age: $c_2^* = 0.24$

Group 3: [30, 50)

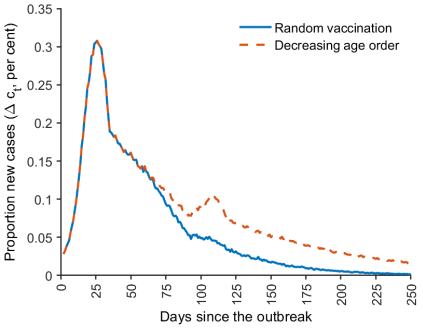

Random: $c_3^* = 0.16$
By age: $c_3^* = 0.23$

Group 4: [50, 65)

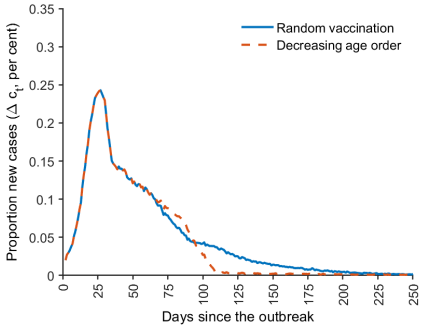

Random: $c_4^* = 0.13$
By age: $c_4^* = 0.12$

Group 5: 65+

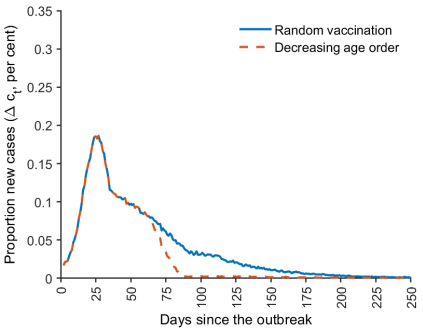

Random: $c_5^* = 0.10$
By age: $c_5^* = 0.08$

Aggregate

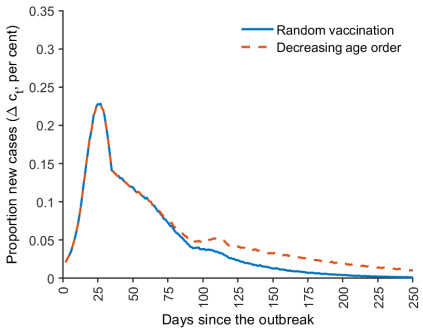

Random: $c^* = 0.12$
By age: $c^* = 0.15$

Notes: The average number of new cases over $B = 1,000$ replications is displayed. Population size is $n = 10,000$. The time profile of β_t/γ under social distancing is displayed in Figure S.13. The vaccination starts during the last month of social distancing (i.e., the 10^{th} week after the outbreak). 50 percent of the population is vaccinated over eight weeks. The vaccine efficacy is $\epsilon_v = 0.95$. The duration of the epidemic is $T^* = 270$ days under random vaccination, and $T^* = 380$ days under vaccination by decreasing age order. $c_\ell^* = B^{-1} \sum_{b=1}^{B} \max_t c_{\ell t}^{(b)}$, for $\ell = 1, 2, \ldots, 5$, and $c^* = B^{-1} \sum_{b=1}^{B} \max_t c_t^{(b)}$.

contrast, the random vaccination strategy would increase the duration from 215 to 270 days.

S7.2 Counterfactual outcomes of early interventions in UK and Germany

To complement Figure 7 presented in the main paper assuming that the German (UK) lockdown had been delayed (brought forward) one week, we further examine the potential outcomes if the lockdown had been delayed or advanced two weeks. As shown in Figure S.16, if the German lockdown had been delayed one week, there would have been a whopping five-fold increase in both infected and active cases. By contrast, if the UK lockdown had been implemented two weeks earlier, both infected and active cases could have been one-fifth of the realized level. These results further highlight the importance of taking mitigation actions early in an epidemic outbreak.

S8 Data Sources

This section provides sources of all the data used in our study. For the multigroup model, the latest population estimates by age for Germany are sourced from the database of the Federal Statistical Office of Germany at `https://www-genesis.destatis.de/genesis/online`. The large-scale social contact surveys by Mossong et al. (2008) provides detailed information on the contact patterns in Germany, and the age-specific contact matrix can be conveniently constructed using the Social Contact Rates (SOCRATES) Data Tool by Willem et al. (2020) available at `https://lwillem.shinyapps.io/socrates_rshiny/`. The data on Germany's Covid-19 cases by age group are retrieved from the website of the Robert Koch Institute at `http://www.rki.de/covid-19-altersverteilung`.

In matching the model with empirical evidence, the primary data source for the Covid-19 cases is the repository by the Center for Systems Science and Engineering (CSSE) at Johns Hopkins University available at `https://github.com/CSSEGISandData/COVID-19`. The Covid-19 cases for each state in the US were aggregated from the county-level data, also available at the CSSE's repository. Since the CSSE data for France and Spain contain negative new

cases at the time of our access, for these two countries we used the data compiled by the World Health Organization available at https://covid19.who.int/WHO-COVID-19-global-data.csv. The population data (for year 2019) are obtained from the World Bank database at https://data.worldbank.org/indicator/SP.POP.TOTL. The lockdown dates across countries can be found at https://en.wikipedia.org/wiki/COVID-19_pandemic_lockdowns.

The efficacy rates of the Pfizer-BioNTech, Moderna, and Johnson & Johnson vaccines are reported in the CDC's Morbidity and Mortality Weekly Reports by Oliver et al. (2020), Oliver et al. (2021), and Oliver et al. (2021), respectively. The shares of people fully vaccinated are sourced from the Our World in Data Covid vaccination dataset at https://github.com/owid/covid-19-data/tree/master/public/data/vaccinations/.

Figure S.16: Counterfactual number of infected and active cases for Germany and UK under different lockdown scenarios

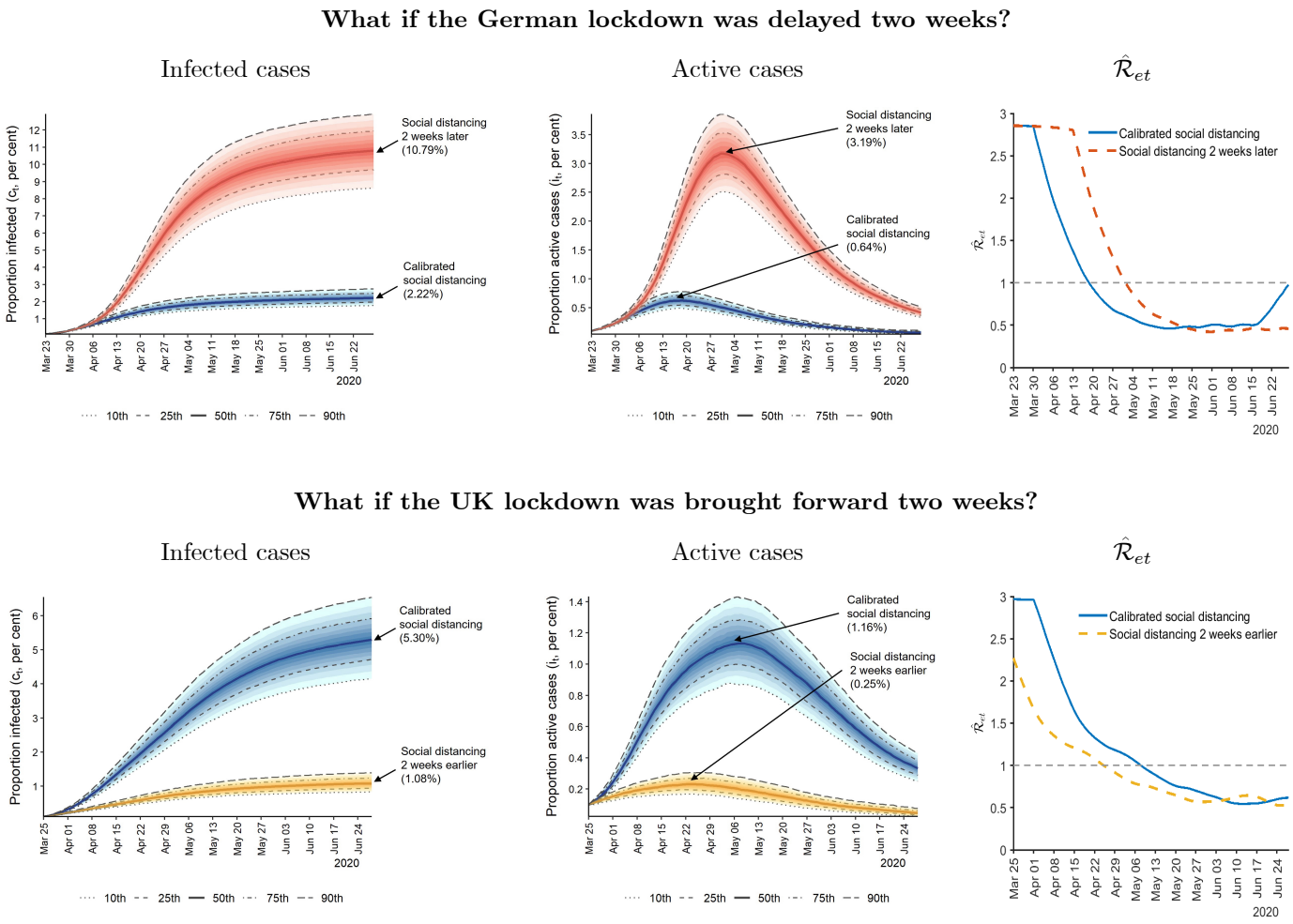

Notes: The simulation uses the single group model with the Erdős-Rényi random network and begins with 1/1000 of the population randomly infected on day 1. The population size used in the simulation is $n = 50,000$. The recover rate is $\gamma = 1/14$. The number of removed (recoveries + deaths) is estimated recursively using $\tilde{R}_t = (1-\gamma)\,\tilde{R}_{t-1} + \gamma \tilde{C}_{t-1}$ for both countries, with $\tilde{C}_1 = \tilde{R}_1 = 0$, where $\tilde{C}_t$ is the reported number of infections. $\hat{\beta}_t$ is the 2-weekly rolling estimate computed by (49) assuming MF = 5. The mean of $\hat{\mathcal{R}}_{et}^{(b)} = \left(1 - c_t^{(b)}\right)\hat{\beta}_t/\gamma$, for $b = 1, 2, \ldots, 1000$ replications, is displayed in the last column.

References

Acemoglu, D., V. Chernozhukov, I. Werning, and M. D. Whinston (2021). Optimal targeted lockdowns in a multi-group SIR model. *American Economic Review: Insights (forthcoming)*.

Akbarpour, M., C. Cook, A. Marzuoli, S. Mongey, A. Nagaraj, M. Saccarola, P. Tebaldi, S. Vasserman, and H. Yang (2020). Socioeconomic network heterogeneity and pandemic policy response. University of Chicago, Becker Friedman Institute for Economics Working Paper No. 2020-75.

Atkeson, A., K. A. Kopecky, and T. A. Zha (2020). Estimating and forecasting disease scenarios for COVID-19 with an SIR model. NBER Working Paper No. 27335.

Baqaee, D., E. Farhi, M. Mina, and J. H. Stock (2020). Policies for a second wave. *Brookings Papers on Economic Activity* (2), 385–443.

Beretta, E. and V. Capasso (1986). Global stability results for a multigroup SIR epidemic model. In T. G. Hallam, L. J. Gross, and A. Levin S (Eds.), *Mathematical Ecology*, pp. 317–340. World Scientific.

Berkane, S., I. Harizi, and A. Tayebi (2021). Modeling the effect of population-wide vaccination on the evolution of COVID-19 epidemic in Canada. medRxiv preprint doi: 10.1101/2021.02.05.21250572.

Bollobás, B. (1980). A probabilistic proof of an asymptotic formula for the number of labelled regular graphs. *European Journal of Combinatorics 1*(4), 311–316.

Chowell, G. and H. Nishiura (2008). Quantifying the transmission potential of pandemic influenza. *Physics of Life Reviews 5*(1), 50–77.

Chudik, A., M. H. Pesaran, and A. Rebucci (2021). COVID-19 time-varying reproduction numbers worldwide: An empirical analysis of mandatory and voluntary social distancing. NBER working paper No. 28629.

D'Arienzo, M. and A. Coniglio (2020). Assessment of the SARS-CoV-2 basic reproduction number, R0, based on the early phase of COVID-19 outbreak in Italy. *Biosafety and Health 2*(2), 57–59.

Dashtbali, M. and M. Mirzaie (2021). A compartmental model that predicts the effect of social distancing and vaccination on controlling COVID-19. *Scientific Reports 11*(1), 1–11.

Ding, D., W. Qin, and X. Ding (2015). Lyapunov functions and global stability for a discretized multigroup SIR epidemic model. *Discrete & Continuous Dynamical Systems-B 20*(7), 1971.

Elliott, S. and C. Gourieroux (2020). Uncertainty on the reproduction ratio in the SIR model. arXiv preprint: 2012.11542.

Ferguson, N., D. Laydon, G. Nedjati Gilani, N. Imai, K. Ainslie, M. Baguelin, ..., and A. C. Ghani (2020). Impact of non-pharmaceutical interventions (NPIs) to reduce COVID-19 mortality and healthcare demand. Imperial College working paper.

Fernández-Villaverde, J. and C. I. Jones (2020). Estimating and simulating a SIRD model of COVID-19 for many countries, states, and cities. NBER working paper No. 27128.

Gourieroux, C. and J. Jasiak (2020). Analysis of virus transmission: A stochastic transition model representation of epidemiological models. *Annals of Economics and Statistics* (140), 1–26.

Guo, H., M. Y. Li, and Z. Shuai (2006). Global stability of the endemic equilibrium of multigroup SIR epidemic models. *Canadian Applied Mathematics Quarterly 14*(3), 259–284.

Harris, J. E. (2020). Overcoming reporting delays is critical to timely epidemic monitoring: The case of COVID-19 in New York City. medRxiv preprint doi: 10.1101/2020.08.02.20159418.

Havers, F. P., C. Reed, T. Lim, J. M. Montgomery, J. D. Klena, A. J. Hall, ..., and N. J. Thornburg (2020). Seroprevalence of antibodies to SARS-CoV-2 in 10 sites in the United States, March 23-May 12, 2020. *JAMA Internal Medicine 180*(12), 1576–1586.

Heffernan, J. M., R. J. Smith, and L. M. Wahl (2005). Perspectives on the basic reproductive ratio. *Journal of the Royal Society Interface 2*(4), 281–293.

Hethcote, H. W. (1978). An immunization model for a heterogeneous population. *Theoretical Population Biology 14*(3), 338–349.

Hethcote, H. W. (2000). The mathematics of infectious diseases. *SIAM Review 42*(4), 599–653.

Hoang, T., P. Coletti, A. Melegaro, J. Wallinga, C. G. Grijalva, J. W. Edmunds, P. Beutels, and N. Hens (2019). A systematic review of social contact surveys to inform transmission models of close-contact infections. *Epidemiology (Cambridge, Mass.) 30*(5), 723.

Hyman, J. M., J. Li, and E. A. Stanley (1999). The differential infectivity and staged progression models for the transmission of HIV. *Mathematical Biosciences 155*(2), 77–109.

Jagodnik, K., F. Ray, F. M. Giorgi, and A. Lachmann (2020). Correcting under-reported COVID-19 case numbers: estimating the true scale of the pandemic. medRxiv preprint doi: 10.1101/2020.03.14.20036178.

Jarvis, C. I., K. Van Zandvoort, A. Gimma, K. Prem, P. Klepac, G. J. Rubin, and W. J. Edmunds (2020). Quantifying the impact of physical distance measures on the transmission of COVID-19 in the UK. *BMC Medicine 18*, 1–10.

Ji, C., D. Jiang, and N. Shi (2011). Multigroup SIR epidemic model with stochastic perturbation. *Physica A: Statistical Mechanics and its Applications 390*(10), 1747–1762.

Kalish, H., C. Klumpp-Thomas, S. Hunsberger, H. A. Baus, M. P. Fay, N. Siripong, ..., and K. Sadtler (2021). Undiagnosed SARS-CoV-2 seropositivity during the first six months of the COVID-19 pandemic in the United States. *Science Translational Medicine 13*(601), 1–11.

Kermack, W. and A. McKendrick (1927). A contribution to the mathematical theory of epidemics. *Proceedings of the Royal Society of London. Series A. 115*(772), 700–721.

Kiss, I. Z., J. C. Miller, and P. L. Simon (2017). *Mathematics of epidemics on networks*, Volume 598. Springer.

Korolev, I. (2021). Identification and estimation of the SEIRD epidemic model for COVID-19. *Journal of Econometrics 220*(1), 63–85.

Lajmanovich, A. and J. A. Yorke (1976). A deterministic model for gonorrhea in a nonhomogeneous population. *Mathematical Biosciences 28*(3-4), 221–236.

Lee, C. and D. J. Wilkinson (2019). A review of stochastic block models and extensions for graph clustering. *Applied Network Science 4*(1), 122.

Leung, K., M. Jit, E. H. Lau, and J. T. Wu (2017). Social contact patterns relevant to the spread of respiratory infectious diseases in Hong Kong. *Scientific Reports 7*(1), 1–12.

Li, M. Y., Z. Shuai, and C. Wang (2010). Global stability of multi-group epidemic models with distributed delays. *Journal of Mathematical Analysis and Applications 361*(1), 38–47.

Li, R., S. Pei, B. Chen, Y. Song, T. Zhang, W. Yang, and J. Shaman (2020). Substantial undocumented infection facilitates the rapid dissemination of novel coronavirus (SARS-CoV-2). *Science 368*(6490), 489–493.

Matrajt, L. and T. Leung (2020). Evaluating the effectiveness of social distancing interventions to delay or flatten the epidemic curve of coronavirus disease. *Emerging Infectious Diseases 26*(8), 1740.

Miller, J. C. and I. Z. Kiss (2014). Epidemic spread in networks: Existing methods and current challenges. *Mathematical Modelling of Natural Phenomena 9*(2), 4–42.

Mossong, J., N. Hens, M. Jit, P. Beutels, K. Auranen, R. Mikolajczyk, ..., and W. J. Edmunds (2008). Social contacts and mixing patterns relevant to the spread of infectious diseases. *PLoS Med 5*(3), e74.

Nepomuceno, E., D. F. Resende, and M. J. Lacerda (2018). A survey of the individual-based model applied in biomedical and epidemiology. *Journal of Biomedical Research and Reviews 1*(1), 11–24.

Newman, M. (2018). *Networks*. Oxford University Press.

Nikbakht, R., M. R. Baneshi, A. Bahrampour, and A. Hosseinnataj (2019). Comparison of methods to estimate basic reproduction number (R0) of influenza, using Canada 2009 and 2017-18 A (H1N1) data. *Journal of Research in Medical Sciences 24*(1), 1–67.

Obadia, T., R. Haneef, and P.-Y. Boëlle (2012). The R0 package: A toolbox to estimate reproduction numbers for epidemic outbreaks. *BMC Medical Informatics and Decision Making 12*(1), 1–9.

Oliver, S., J. Gargano, M. Marin, M. Wallace, K. G. Curran, M. Chamberland, ..., and K. Dooling (2020). The advisory committee on immunization practices' interim recommendation for use of Pfizer-BioNTech COVID-19 vaccine — United States, December 2020. *MMWR. Morbidity and Mortality Weekly Report 69*(50), 1922–1924.

Oliver, S., J. Gargano, M. Marin, M. Wallace, K. G. Curran, M. Chamberland, ..., and K. Dooling (2021). The advisory committee on immunization practices' interim recommendation for use of Moderna COVID-19 vaccine — United States, December 2020. *MMWR. Morbidity and Mortality Weekly Report 69*(5152), 1653–1656.

Oliver, S. E., J. W. Gargano, H. Scobie, M. Wallace, S. C. Hadler, J. Leung, and . K. Dooling (2021). The advisory committee on immunization practices' interim recommendation for use of Janssen COVID-19 vaccine — United States, February 2021. *MMWR. Morbidity and Mortality Weekly Report 70*(9), 329–332.

Pastor-Satorras, R., C. Castellano, P. Van Mieghem, and A. Vespignani (2015). Epidemic processes in complex networks. *Reviews of Modern Physics 87*(3), 925.

Rahmandad, H., T. Y. Lim, and J. Sterman (2021). Behavioral dynamics of COVID -19: estimating underreporting, multiple waves, and adherence fatigue across 92 nations. *System Dynamics Review 37*(1), 5–31.

Rocha, L. E. and N. Masuda (2016). Individual-based approach to epidemic processes on arbitrary dynamic contact networks. *Scientific Reports 6*, 31456.

Schlickeiser, R. and M. Kröger (2021). Analytical modeling of the temporal evolution of epidemics outbreaks accounting for vaccinations. *Physics 3*(2), 386–426.

Thieme, H. R. (1983). Global asymptotic stability in epidemic models. In H. W. Knobloch and K. Schmitt (Eds.), *Equadiff 82 Proceedings*, pp. 608–615. Springer.

Thieme, H. R. (1985). Local stability in epidemic models for heterogeneous populations. In V. Capasso, E. Grosso, and S. L. Paveri-Fontana (Eds.), *Mathematics in Biology and Medicine*, pp. 185–189. Springer.

Thieme, H. R. (2013). *Mathematics in population biology*, Volume 12 of *Princeton Series in Theoretical and Computational Biology*. Princeton University Press.

Toda, A. A. (2020). Susceptible-infected-recovered (SIR) dynamics of COVID-19 and economic impact. arXiv preprint: 2003.11221.

Willem, L., T. Van Hoang, S. Funk, P. Coletti, P. Beutels, and N. Hens (2020). SOCRATES: An online tool leveraging a social contact data sharing initiative to assess mitigation strategies for COVID-19. *BMC Research Notes 13*(1), 1–8.

Willem, L., F. Verelst, J. Bilcke, N. Hens, and P. Beutels (2017). Lessons from a decade of individual-based models for infectious disease transmission: A systematic review (2006–2015). *BMC infectious diseases 17*(1), 612.

Zhang, J., P. Klepac, J. M. Read, A. Rosello, X. Wang, S. Lai, ..., and H. Yu (2019). Patterns of human social contact and contact with animals in Shanghai, China. *Scientific Reports 9*(1), 1–11.

Zhang, J., M. Litvinova, Y. Liang, Y. Wang, W. Wang, S. Zhao, ..., and H. Yu (2020). Changes in contact patterns shape the dynamics of the COVID-19 outbreak in China. *Science 368*(6498), 1481–1486.

Zhou, J., Y. Yang, and T. Zhang (2017). Global stability of a discrete multigroup SIR model with nonlinear incidence rate. *Mathematical Methods in the Applied Sciences 40*(14), 5370–5379.